

A review of printing strategies, sustainable cementitious materials and characterization methods in the context of extrusion-based 3D concrete printing

Chen, Yu; He, Shan; Gan, Yidong; Çopuroğlu, Oğuzhan; Veer, Fred; Schlangen, Erik

DOI

[10.1016/j.jobe.2021.103599](https://doi.org/10.1016/j.jobe.2021.103599)

Publication date

2022

Document Version

Final published version

Published in

Journal of Building Engineering

Citation (APA)

Chen, Y., He, S., Gan, Y., Çopuroğlu, O., Veer, F., & Schlangen, E. (2022). A review of printing strategies, sustainable cementitious materials and characterization methods in the context of extrusion-based 3D concrete printing. *Journal of Building Engineering*, 45, Article 103599.
<https://doi.org/10.1016/j.jobe.2021.103599>

Important note

To cite this publication, please use the final published version (if applicable).
Please check the document version above.

Copyright

Other than for strictly personal use, it is not permitted to download, forward or distribute the text or part of it, without the consent of the author(s) and/or copyright holder(s), unless the work is under an open content license such as Creative Commons.

Takedown policy

Please contact us and provide details if you believe this document breaches copyrights.
We will remove access to the work immediately and investigate your claim.

Contents lists available at [ScienceDirect](https://www.sciencedirect.com)

Journal of Building Engineering

journal homepage: www.elsevier.com/locate/job

A review of printing strategies, sustainable cementitious materials and characterization methods in the context of extrusion-based 3D concrete printing

Yu Chen^{a,*}, Shan He^a, Yidong Gan^a, Oğuzhan Çopuroğlu^a, Fred Veer^b, Erik Schlangen^a

^a *Microlab, Faculty of Civil Engineering and Geosciences, Delft University of Technology, Delft, the Netherlands*

^b *Faculty of Architecture, Delft University of Technology, Delft, the Netherlands*

ARTICLE INFO

Keywords:

3D concrete printing
 Printing strategy
 Sustainable cementitious material
 3D printable behavior
 Fresh property
 Interlayer
 Test method

ABSTRACT

This paper aims to provide a systematical review of the available printing strategies, sustainable cementitious materials and characterization methods for extrusion-based 3D concrete printing (3DCP). The printing strategies, consisting of printing setup, process, and material requirements, were summarized initially. In the material aspect, the high ordinary Portland cement (OPC) content in most printable mixtures is a major issue that impedes the sustainability of 3DCP. This can be resolved by partially substituting OPC with supplementary cementitious materials (SCMs). In this review, the effect of different SCMs on fresh-state behaviors and 3D printing of cementitious materials was comprehensively discussed. Finally, a series of test methods for quantitatively characterizing fresh properties, 3D printability and interlayer behaviors were summarized and reviewed.

1. Introduction

Over the past decade, there has been a dramatic development in the research of extrusion-based 3D concrete printing (3DCP) [1–3]. Recently, considerable literature has grown up around this theme. The process of 3DCP is that filaments of cementitious materials are extruded and deposited based on 3D model data to form components without formwork [4,5]. According to Refs. [6–8], 3DCP can be considered as a sustainable construction approach of concrete. The use of 3DCP may bring many benefits to reduce environmental impacts due to concrete construction. First, elimination of formwork reduces the construction time, cost, labor, material, and waste generation [9,10]. Second, combined with topology-optimized structural design methods, 3DCP becomes a more sustainable fabrication method in practice [6,11]. About 50% of environmental impact can be reduced by employing additive manufacturing of concrete combined with structural optimization compared to conventional construction [12,13]. Finally, sustainable cementitious materials are feasible to be used in 3DCP. Many recent studies attempted to develop such materials by employing different approaches, for instance, partially replacing ordinary Portland cement (OPC) by supplementary cementitious materials (SCMs) [14–18], partially substituting natural aggregate by recycled aggregate [19–21], or with other industrial wastes [22,23]. However, to date, the way to enhance the sustainability of 3DCP, especially within the context of using low OPC (SCMs-based) binders in printable cementi-

* Corresponding author.

E-mail addresses: Y.Chen-6@tudelft.nl (Y. Chen), S.He-2@tudelft.nl (S. He), Y.Gan@tudelft.nl (Y. Gan), O.Copuroglu@tudelft.nl (O. Çopuroğlu), F.A.Veer@tudelft.nl (F. Veer), Erik.Schlangen@tudelft.nl (E. Schlangen).

<https://doi.org/10.1016/j.job.2021.103599>

Received 19 February 2021; Received in revised form 9 August 2021; Accepted 5 November 2021

Available online 11 November 2021

2352-7102/© 2021 The Authors. Published by Elsevier Ltd. This is an open access article under the CC BY-NC-ND license

(<http://creativecommons.org/licenses/by-nc-nd/4.0/>).

tious materials, has not been adequately summarized. Additionally, there is a lack of comprehensive review about the influences of different SCMs on the rheology and 3D printability of fresh cementitious materials.

Many distinct fresh-state behaviors, e.g., pumpability, extrudability, and buildability, are required in 3DCP [24,25]. These material behaviors are primarily constrained by the printing strategy, i.e., the printing system and process. Generally, 3D printable cementitious materials should be formulated compatible with the printing strategy. In addition, the methods for investigating the fresh and hardened properties of conventional cementitious materials did not satisfy the demands for quantifying and developing 3D printable cementitious materials. Many modified or novel methods that were proposed in this context, therefore, need to be summarized. For a comprehensive demonstration of state-of-the-art review on 3D printable cementitious materials, all the above-mentioned aspects should be taken into consideration.

The goal of this study is to systematically review and discuss the printing strategies, sustainable cementitious materials, and characterization methods for 3DCP. This work will be helpful to material researchers for a better understanding of 3DCP. Therefore, this paper was organized into three distinct parts. The first part explored the available printing strategies. In the second part, a comprehensive review of the low OPC (SCMs-based) binders used in the available 3D printable cementitious materials was presented. The influences of different SCMs on the rheology and 3D printing of fresh mixtures were highlighted and discussed. Finally, the test methods for characterizing the fresh properties and interlayer behaviors of 3D printed cementitious materials were summarized.

Note that the authors focused on specific issues and research interests rather than attempting to give all processes, materials and tests related to 3DCP in this paper. Thus, the scope and limitation of this work must be clarified: (1) extrusion-based printing technique is the only digital construction method reviewed here; (2) sustainable cementitious materials represent the SCMs-based blended cementitious materials (alkali-activated binders and low clinker cements, e.g., calcium sulfoaluminate cement, and calcium aluminate cement, are excluded); (3) the characterization methods only include the tests about fresh state behaviors (flowability, rheology, and stiffness evolution), 3D printability and interlayer bonding properties.

2. Extrusion-based 3D concrete printing strategy

Most of the 3DCP systems being used in both academic institutes and construction industry consist of three primary units: a deposition setup, a control unit, and a material conveying system. Both 3- or 4-axis gantry-based and 6-axis robotic deposition setups were implemented [26]. The deposition setup is controlled by the control unit to fulfill a predefined printing path that is programmed by the operator. There are at least 3 translational degrees of freedom (DOF) in the gantry-based deposition setups, e.g., x-, y-, and z-plane. For the 4-axis gantry robot, a 4th DOF is attached on the z-axis (vertical direction) to provide a rotation. Compared to 3- and 4-axis gantry-based deposition setups, industrial robotic arms can exhibit up to 6 rotational DOF [27], which can help to print more complex geometries. However, controlling 3- and 4-axis gantry-based deposition setups may be much easier than 6-axis robot arms. The material conveying system may comprise a series of components, i.e., a mixing machine, a pump, a printhead, and others, for preparing, pumping, and extruding the fresh mixtures.

In material preparation, there are two main strategies, as mentioned by Wolfs [27]. First, the fresh mixture is mixed in multiple batches and hereafter delivered manually or automated to the hopper of the material conveying pump (see Fig. 1 (a)). This approach is mainly preferred in a small-scale application, e.g., printable material development and other experimental activities. Second, a continuous system, such as an inline mixing machine that works with the pump synchronously (see Fig. 1 (b)), is required for large-scale construction. The various mixing strategies may lead to different demands on fresh mixtures. For example, the former may require fresh mixtures with a relatively longer open time/printability window than the latter. However, it also depends on the hose length and material flow rate. Due to the short and intense mixing procedures, the inline mixing approach may not be a proper way for preparing certain fresh mixtures containing a high dosage of fibers and/or exhibiting high yield stress and viscosity during the mixing process. There are still some discussions concerning which strategy would be the most appropriate. In different cases, the size of each batch and the mixing strategy are primarily dependent on factors, e.g., the geometry of printed component, volume deposition rate (material flow rate), and open time of the printing material [1].

In many cases, the pumping and extrusion forces are generally supplied by a ram extruder or a material conveying pump on the basis of a rotor-stator configuration (see Fig. 1 (a) (b)). The printhead could be a simple nozzle that has the rectangle opening (most time) with or without a geometric reduction. Roussel [28] mentioned that the shear force between fresh mixtures and the inner wall of hose and nozzle is concentrated at the interface that is also regarded as the lubrication layer. The ability to form the lubrication layer of fresh mixtures becomes critical to evaluate its pumpability and extrudability. During the pumping and extrusion process, a plug zone might exist where the material may already be flocculated and exhibits a certain yield stress. Therefore, the material showed high/sufficient stiffness and near zero-slump after deposition from the nozzle. This strategy is classified as the extrusion of high or sufficiently stiff materials in Mechtcherine et al. [2].

However, it should be noted that the pumping distance (hose length) for extrusion of stiff materials is limited due to the high pumping pressure induced by the high yield stress and plastic viscosity (leading to a significant increase of material temperature and a short initial setting time). Thus, the extrusion of flowable material is proposed as a superior strategy for 3DCP. The material exhibits exceptionally high fluidity, requiring significantly lower pump pressure and energy input than the high/sufficiently stiff material during the mixing, pumping, and extrusion processes. However, once the flowable material is deposited from the nozzle, it should reach sufficient stiffness rapidly. Enhancing the stiffness of the flowable mixture within a short time is quite critical in this context. Rheology-/hydration-control (or set on-demand) as a proper way is therefore proposed by many researchers [13,31–33]. Accelerating the stiffness of material during and after deposition is the main idea of this strategy. As mentioned by Mechtcherine et al. [2], the principle of this strategy is to mix “active agent”, which could be a chemical accelerator, an organic rheology modifier, or a kind of fast-set

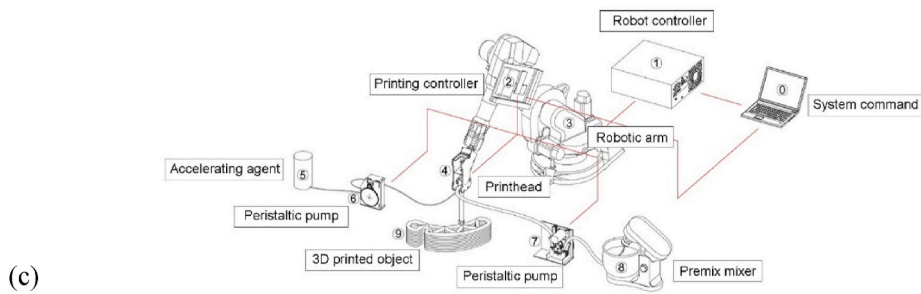
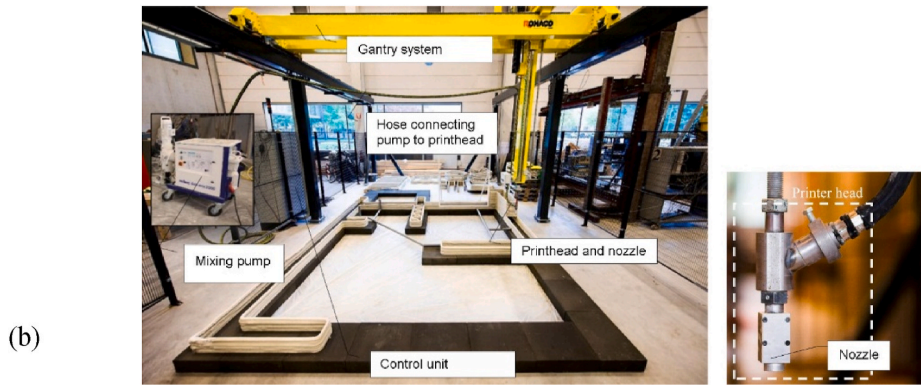
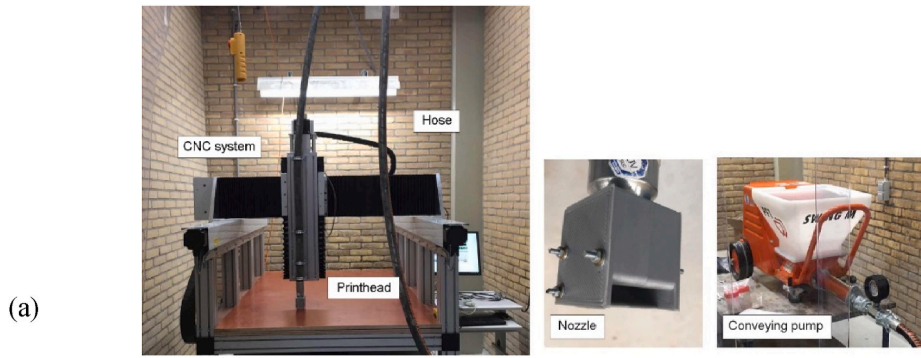


Fig. 1. Typical 3DCP experimental setups. (a) TU Delft: 3-axis gantry-based system, multiple batches (material preparation), and rotor-stator-based pump, adapted from Ref. [26]; (b) TU Eindhoven: 4-axis gantry-based system, continuous mixing (material preparation), and rotor-stator-based pump, adapted from Ref. [29]; (c) XtreeE: 6-axis robotic arm, peristaltic pump, and inline mixing and extrusion printhead (set-on-demand), adapted from Ref. [30]; (d) TU Dresden: 4-axis gantry-based system, multiple batches, and screw extruder, adapted from Ref. [3].

cement slurry (such as aluminate-based cement [34]), with the fresh mixture in the printhead (see Fig. 1 (c)). To achieve the goal of this strategy, it largely depends on the dispersion/mixing of “active agent” and the design of the printhead. Earlier attempts of this strategy were made by Refs. [30,31,35,36]. On the other hand, the pumping process may be excluded in several 3DCP systems that only consist of a large volume of V-shape material hopper and a screw extruder (see Fig. 1 (d)). The prepared fresh mixture is poured into the hopper directly. Dependent on the gravitational flow with or without the additional energy input (which depends on the fluidity of fresh mixtures), the material is transported to the bottom of the hopper, where the screw extruder is positioned.

3. SCM-based cementitious materials for 3DCP

Technically, most available 3D printable cementitious materials are designed in the form of grout and mortar as typically fine aggregate (grain size < 2 mm) is employed. 3D printable cementitious materials in this study are mainly referred to as printable mortars that primarily contain three components: binder, fine aggregate, and water. The manufacturing process of OPC, which consumes large quantities of resources and energy, and generates massive amounts of greenhouse gases, results in a substantial burden on our living environment [6,37]. Cement industry is responsible for 5–7% of the global anthropogenic CO₂ emission [38,39]. Compared to mold-cast concrete, 3D printable cementitious materials may require a much higher amount of OPC. As shown in Fig. 2, the proportion of OPC in most of the 3D printable cementitious materials is more than 20 wt%. Assuming a typical concrete mixture's unit weight is 2200 kg/m³, the majority of printable mixtures would contain at least 330 kg/m³ of OPC. In Fig. 2, the aggregate to binder mass ratio (A/B) is smaller than 2 in most of printable mixtures, whereas the A/B is of the order 3–3.5 in high strength mold-cast concrete (equal or greater than 60 MPa of compressive strength at 28 days), and more than 5 in moderate strength mold-cast concrete (about 30 MPa of compressive strength at 28 days) [40].

There are two strategies for developing low OPC-content cementitious materials in the field of 3DCP: (1) Use supplementary cementitious materials (SCMs) or other types of low carbon cement to substitute a high volume of OPC; (2) Reduce the binder content by increasing the proportion of aggregate (the binder composition is fixed). This study focuses on the cement replacement strategy, while the reader could refer to works [25,41,42] for the A/B modification strategy.

3.1. Effect of common SCMs

Common SCMs, including fly ash, blast furnace slag, and silica fume, have been used as a partial replacement of OPC/clinker in 3D printable cementitious materials [6,8,57]. The initial idea of using such SCMs in printable mixtures is to improve the packing density, cohesion, and flow consistency. The addition of SCMs can significantly influence the rheological behavior of fresh mixtures. However, for different SCMs, the impacts on fresh properties may not be the same, as shown in Table 1.

Depending on the coal composition, fly ash can be distinguished as siliceous (Class F) and calcareous (Class C) types [58]. Compared to siliceous fly ash, calcareous fly ash contains a much higher content of reactive CaO, which could enable self-cementitious properties [58–60]. In this paper, fly ash (FA) is referred to as siliceous/Class F fly ash as it was mainly used in the available printable cementitious materials. For example, Panda et al. [43,48,55,56] proposed many 3D printable cementitious materials containing a high volume of FA. Up to 80% of OPC in the binder mass was replaced by FA in their study [48]. FA particles having high sphericity and smooth surface texture improve the flowability of self-compacting concrete [61,62]. Due to the “ball bearing effect”, replacing a high amount of OPC by FA may reduce the yield stress and plastic viscosity [63], which could contribute to the pumpability of fresh mixtures. However, the unburnt coal in FA could adsorb superplasticizer or the mixing water, which may affect the workability of

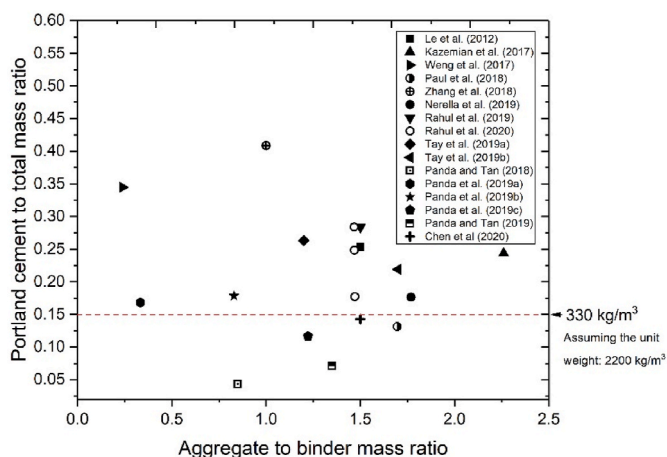


Fig. 2. Literature survey of OPC content and aggregate to binder mass ratio in different 3D printable mortars. Data from Refs: [25,26,43–56].

Table 1
Material characteristics of different SCMs [61,66,91].

	Fly ash (siliceous)	Silica fume	Granulated blast furnace slag	Limestone	Calcined clay (Metakaolin as the main phase)
Material type	By-product	By-product	By-product	Natural material	Calcined natural SCMs
Morphology	Round particle and smooth surface	Round particle	Finely granular particle and smooth surface	Irregular shape and rough surface	Layered structure and rough surface
Fineness [μm]	10-150 (may coarser than cement particles)	0.01-0.5.	3-100 (close to cement particles)	Close to/finer than that of cement particles (depends on the grinding process)	Generally, finer than other SCMs except for SF.
Specific gravity [g/cm^3]	~ 2.1	~ 2.2	~ 2.9	~ 2.7	2.1–2.5
Chemistry (phase compositions)	Si–Al–O	Si–O	Ca–Si–Al–Mg–O	CaCO_3	Si–Al–O
The maximum proportion of the binder mass in printable mixtures	80% [48].	20% [47].	85% [49]	55% [92]	40% [26]
The main effect on rheological behaviors	(1) The ball-bearing effect could improve flowability and reduce yield stress and plastic viscosity. (2) Dilution effect on cement flocculation (high volume replacement).	(1) Generally, it could increase the yield stress and plastic viscosity. (2) It could enhance the flocculation of cement particles, resulting in improved buildability and structural build-up of fresh mixtures.	(1) GGBS with a smooth particle surface and low reactivity can improve the workability, and reduce plastic viscosity and/or yield stress. (2) Workability may be negatively affected by the GGBS with high SSA and reactivity.	(1) Limestone with coarser or similar particle size compared to cement could reduce the yield stress and plastic viscosity for improving workability. (2) The opposite effect can be obtained by using ultrafine limestone.	(1) Generally, it could reduce the workability and increase the yield stress and plastic viscosity. (2) The structural build-up/thixotropic behaviors can be enhanced.
The main effect on hydration	Pozzolanic	Filler effect and pozzolanic	Latent hydraulic	Filler effect	Filler effect (may be for small MK replacement) and pozzolanic
Estimated total amount [Mt/year]	700–1100	1–2.5	300–360	Abundant accessible reserves	Abundant accessible reserves

fresh mixtures [61]. On the other hand, FA shows similar or relatively coarser particle size and smaller density than OPC. Using a high volume of FA in the binding material could result in a significant dilution effect, i.e., reducing the number of cement particle flocs, adversely affecting structural build-up, delaying the initial setting and early hydration [15,61]. For improving the structural build-up of such blended mixtures, other SCMs, like silica fume/micro-silica [50,64], could be used to formulate the ternary binder system (cement-FA-silica fume) for 3DCP. Additionally, adding admixtures, e.g., nano attapulgite clay, and methyl cellulose-based viscosity modifying admixture (VMA), can also enhance the robustness and thixotropy of such high volume of FA based printable cementitious materials [43,52,56,65]. Besides, it should be noted that replacing OPC with a very high volume of FA (more than 50 wt% of binder) may require alkalinization for the setting and hardening process. The general approaches for activating FA-based binders included: grinding FA (for increasing specific surface area and reducing fineness), introducing a small content of highly reactive materials (e.g., silica fume), and adding a proper dosage of chemical activator [15,58]. Panda et al. [55,56] added about 3 wt% (of binder) sodium sulfate as activating agent to enhance the early strength of their high-volume FA based printable cementitious materials.

Granulated blast furnace slag (GBFS) is also a very commonly used and valuable SCM. For achieving good reactivity, slag is further ground to a fineness comparable to cement particles [66,67]. Due to its latent hydraulic property, ground granulated blast furnace slag (GGBS) can replace up to 95% of clinker in European CEM III/C cement, according to EN 197-1 [68]. Due to the micro-filling effect, the workability may be improved by increasing OPC substitution using GGBS [58,61,67]. However, the effect of GGBS on the rheology of fresh mixtures is mostly dependent on its physical and chemical properties. Compared to OPC, the GGBS with smooth particle surface and low reactivity could improve workability, resulting in decreased plastic viscosity and/or yield stress (see Refs. [69,70]). In contrast, the water and superplasticizer demands are increased by using the GGBS that has a relatively high specific surface area (SSA) and chemical reactivity [61]. Currently, there are only a few attempts to develop GGBS-based cementitious materials for 3DCP. Panda et al. [49] investigated the rheology, 3D printability, and compressive strength of ternary blends containing GGBS, cement, and lime. Their work confirmed that it is possible to employ a high volume of slag (70–85 wt% of binder) in 3D printable cementitious materials. Rahul et al. [46] studied desorptivity of a GGBS-based cementitious material (50% of GGBS in binder) for 3DCP. Chaves Figueiredo et al. [65] developed a series of printable strain-hardening cementitious composites that comprise GGBS, OPC, and limestone. Nevertheless, most of the studies [7,71–76] in literature have focused on developing alkali-activated slag-

or slag and fly ash-based geopolymer materials for 3D printing, which is beyond the scope of this paper, and therefore, is not discussed.

Silica fume (SF) can fill the space between other cementitious particles to increase the packing density and improve the cohesion due to its ultrafine particle size, round shape, and extremely high SSA. The water and superplasticizer demand and inner particle friction are increased by using SF as the constituent of binder [61,77–80]. Many studies [61,81–84] showed that both yield stress and plastic viscosity are increased upon addition of SF, whereas the opposite results (decrease in yield stress and/or plastic viscosity) were observed in cases [70,85,86]. According to Refs. [61,84,87], this is primarily due to the different physical characteristics (e.g., surface properties, density, and morphology) and volume fraction of SF in different studies. Besides, the effect of SF on rheology is also related to the different water to binder ratio and different types of superplasticizers. The ternary blend appears very frequently in the available mix designs for 3DCP. Such ternary blends may comprise OPC, one of SCMs with moderate particle size (FA, GGBS, or limestone powder), and one of the ultrafine materials, i.e., SF, or other inorganic fines. Examples of these ternary blend systems can be found in Refs. [25,47,52,53,84,88]. SF was used as an SCM addition with up to 20% of binder mass [47] in 3D printable cementitious materials. In this context, SF can improve the flow consistency of fresh mixture for extrusion and enhance the buildability and structural build-up at rest, attributed to the filler effect. As stated by Lothenbach et al. [89], more nucleation sites for the hydration products of cement phases are provided by the fine SCMs, like SF and metakaolin.

For a long-term application, the main challenge with respect to the utilization of common SCMs (FA, GGBS, and SF) is their gradually reducing production and availability [6,8,57,90]. As shown in Table 1, the total amount of SF is only 1–2.5 Mt/year. The quantity of slag is much higher than SF, whereas it is about 5–10% of OPC. Under the environmental pressures, the amount of slag is severely affected by the decrease in iron production due to the increased recycling of steel. The estimated annual production of FA is 700–1100 Mt [66]. However, not all FA is suitable for the use in cement due to quality reasons [90]. Additionally, the supply chain of FA is threatened by reasons such as retirement or elimination of coal-fired power plants in many countries (e.g., the USA, the UK, and the Netherlands) [66]. Finding alternative SCMs appears to be a critical task in order to ensure uninterrupted supply of SCMs-based cementitious materials. Owing to the abundant availability worldwide, (calcined) clay and limestone stand out as the ideal alternatives.

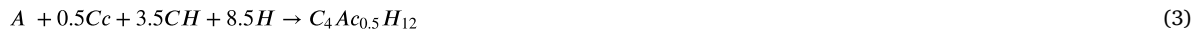
3.2. Effect of limestone and calcined clay

Limestone powder is utilized as a kind of filler component in binding material. Similar to the SCMs mentioned earlier, the effect of limestone on rheology is linked to the physical properties of limestone particles, i.e., fineness and roughness of the surface. These material characteristics strongly affect the packing density and the demand for water and superplasticizer [61]. In the case of limestone powder with similar or coarser fineness compared to that of cement, the addition of limestone may improve workability by reducing yield stress and plastic viscosity [93]. In contrast, such parameters can be increased by using the ultrafine limestone [94] due to the high adsorption of water and superplasticizer, as well as the enhancement of inner particle friction. Also, the cement flocculation may be enhanced and accelerated by decreasing the particle size of limestone (for the fixed limestone proportion) [95] or increasing the volume of limestone (for the fixed fineness of limestone) [83]. Filler effect can be regarded as the main influence of limestone addition on cement hydration, which may relate to two mechanisms: the dilution of cement, and the increase of nucleation sites provided by the limestone surface, as stated by Berodier and Scrivener [96]. Replacing a partial amount of OPC by limestone could accelerate the early age hydration, especially when the average particle size of limestone is very fine, because of the increase of nucleation sites [96]. However, it may affect the mechanical performance and increase the porosity of hardened cementitious materials when the substitution of OPC by limestone alone is higher than 10% in the binder [90,97]. This is attributed to the dilution effect of limestone filler. There are only several examples [92,98] of using limestone as the main substitute of OPC for formatting the binary binder system for 3DCP. Many 3D printable cementitious materials employ a blend of limestone and one or two of SCMs, e.g., GGBS [65,99], SF [30,100], fly ash [65,99], or calcined clay [26,46,57,100,101] as the OPC replacement.

The utilization of calcined clay as an SCM for concrete has attracted much attention in the past decade. The advantages of using calcined clay as the OPC substitute can be summarized as follows.

- (1) The raw materials (clays) are vastly abundant worldwide. As the most suitable type, kaolinitic clay is rich in tropical and subtropical environments, especially in India and Southeast Asia [102].
- (2) The calcination process requires fewer fuels and emits much less CO₂ compared with that of clinker production. The burning temperature is about 700–850 °C for manufacturing calcined clay (around 1450 °C for clinker) [90,103]. The heating time could be controlled within several tenths of a second using flash calcination units [104]. As reported by Huang et al. [105], only 0.25–0.37 kg of CO₂ is emitted by producing 1 kg of calcined clay, which is much less than that for producing 1 kg of OPC (about 0.9 kg of CO₂).
- (3) The ternary blends, containing limestone, calcined clay, and clinker (referred to LC3), were studied by many researchers [106–108]. The most typical one, LC3-50, comprises 50% clinker, 15% limestone, 30% calcined clay, and 5% gypsum. Metakaolin (MK), as the primary reactive phase in calcined clay, is the calcined product of high purity kaolinitic clays. MK, at a relatively high price (near three times of cement), is generally used in other industries, including paper, ceramics, and refractory [90]. According to Refs. [109,110], using the calcined low-grade kaolinitic clay (containing 40% of MK) in LC3-50 cement could reach compressive strength comparable to that of plain OPC from 7 days. Such low-grade kaolinitic clays are also the low-cost raw material for producing cement and probably available around quarries of cement plants [90].
- (4) The amorphous aluminosilicate in MK (AS₂) could react with the calcium hydroxide (CH) for forming aluminates hydrates and C-(A)-S-H (see Eq (1)). Besides, the calcite (Cc) from limestone can react with alumina species (C₃A and A from AS₂) in the pore

solution to generate hemi/mono-carboaluminate ($C_4Ac_{0.5}H_{12}$) (see Eq (2)(3)) for inhibiting formation of ettringite [90,97,103,107,111]. All the aforementioned products could refill the pores and reduce the total porosity, contributing to enhancing the strength and durability of hardened cementitious materials [90,103,112]. Using LC3 could improve the durability of hardened concrete, for example, the excellent chloride resistance [113–116], proper performance under the sulfates attack [117,118], and mitigation of the alkali-silica reaction [90,117,119].



As shown in Fig. 3, clays, without calcination, are categorized according to the way that tetrahedral (Al^{3+} for Si^{4+}) and octahedral (Fe^{3+} , Fe^{2+} , or Mg^{2+} for Al^{3+}) sheets are combined into layered structures. The clay is referred to the 1:1 or t-o clay if only one tetrahedral and one octahedral sheet are available in each layer. The layers are linked by hydrogen bonds. In contrast, the 2:1 or t-o-t clay contains two tetrahedral sheets positioned at both sides of one octahedral sheet. The interlayer electrostatic forces and cations bond the layers in this case [120,121]. Different amounts of water molecules and various types of ions can be hosted at the large interlayer. Induced by the changes of relative humidity, the 2:1 clay may easily swell and shrink. Kaolinite is a typical non-swelling 1:1 clay. For those 2:1 clays, muscovite is a non-swelling clay (in the group of illites), whereas montmorillonite belongs to a swelling clay (in the group of smectites) [121]. Polycarboxylate ethers (PCEs), as the most common superplasticizer, can be significantly adsorbed on the swelling clays, which strongly affects or even nullifies the dispersion of PCEs. Consequently, the other fines in the mixture could not get enough PCEs for achieving the designed workability. However, this is not a critical issue for non-swelling clays [121,122]. The possible mechanisms of PCEs adsorption by swelling clays were explained elsewhere [33]. As mentioned earlier, low-grade kaolinitic clay is recommended to be used for producing LC3. Except for MK, the calcined low-grade kaolinitic clay may contain quartz, limestone, iron-bearing phases, and other calcined/uncalcined clay minerals. Therefore, the characterization of crystalline phases in calcined clay appears to be essential, especially to determine if swelling clays are present. The phase transformation of natural clay under different temperatures is illustrated in Fig. 4. At a relatively low temperature, water from the interlayers of clays is removed. After that, a progressive dehydroxylation process results in removing hydroxyl groups, and layers collapse with increased temperature. The amorphous structure that shows the highest pozzolanic reactivity is formed at this stage. Nevertheless, if exceeding this temperature (850 °C for the kaolinitic clay), the amorphous structure is transformed into a crystalline or glass formation [111]. After calcination under 850 °C, kaolinitic clay transforms into the amorphous phase (MK), whereas 2:1 clays, including illite and montmorillonite, could keep a layered crystalline structure (because the required temperature for 2:1 clays is much higher than 850 °C) [123].

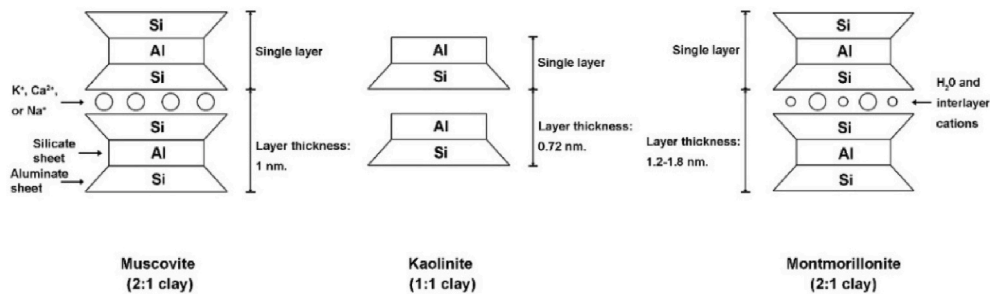


Fig. 3. Diagram showing the structure of muscovite, kaolinite, and montmorillonite, adapted from Ref. [121].

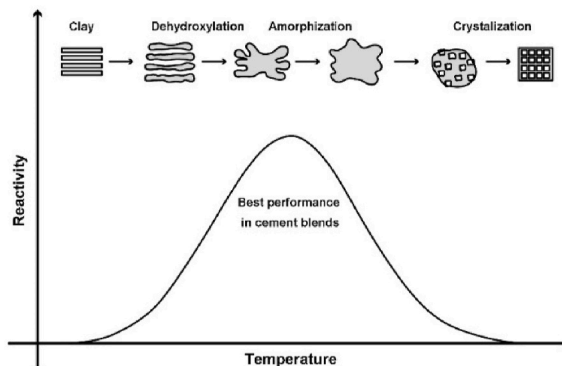


Fig. 4. Clay phases transformation at different calcined temperatures, adapted from Ref. [111].

The addition of calcined clay could generally reduce the workability of fresh cementitious materials [16,93,123], which results in high water and superplasticizer demands [124–126]. However, these impacts on the rheology of fresh mixtures may vary depending on the type of calcined clay used. Calcined clays provided by different suppliers may exhibit various chemical and physical characteristics [116], for example, the different MK contents (40–90%), secondary phase (quartz, limestone, clays, and others), fineness, SSA, morphology, and density. These differences may be induced by different raw materials (2:1 or 1:1 clay), calcination methods (temperatures and devices), cooling, and grinding processes. Ferreiro et al. [127] compared the workability and strength of two calcined clays (calcined 2:1 and 1:1 clays). They reported that adding calcined 1:1 clay (the 1:1 clay contains 92% kaolinite) in mixtures increases the water demand compared with that of calcined 2:1 clay (the 2:1 clay consists of 68% montmorillonite) for archiving the same flowability at a fixed PCE dosage. Studies [123,128] pointed out that the calcined clay containing quartz (even a small amount) could reduce the demands of water and PCEs. Sposito et al. [123] also reported that the SSA, zeta potential, and water demand of calcined clay (except for metamuscovite) could be used to indicate the demand for superplasticizer. In their study, the required dosage of superplasticizer significantly increased with increasing these three indicators' value. The calcination and grinding methods may influence the morphology of calcined clay. The spherical MK particle that was manufactured using a flash calcination method proposed by Claverie et al. [129] could primarily enhance the workability of fresh cementitious materials. On the other hand, Akhlaghi et al. [130] introduced a modified PCE-based superplasticizer that could efficiently disperse mixtures containing a high content of calcined clay and a high concentration of sulfate ions. This superplasticizer may be an ideal option for LC3 or other multi-component cement systems.

Calcined clay is also a good ingredient to improve the structural build-up of fresh mixtures at rest, which could be regarded as an advantage of developing calcined clay-based cementitious materials for 3DCP. According to Muzenda et al. [131], the addition of calcined clay could increase the rheological parameters, i.e., thixotropic index, apparent viscosity, cohesion, static and dynamic yield stresses of fresh pastes. Beigh et al. [132] characterized the static yield stress of LC3 paste at different resting times (23–120 min). They found that the structuration rate of LC3 paste is much higher than that of the reference OPC paste. The enhancement of structural build-up may be attributed to the high SSA and layered particle structure of calcined clay [131]. However, as mentioned earlier, using different calcined clays may result in the various structural build-up of fresh mixtures. For example, Chen et al. [57] reported that increasing the MK content in calcined clay could increase the green strength and decrease the initial setting time of limestone and calcined clay-based cementitious material. Similarly, Aramburo et al. [133] found that the structuration rate of the fresh mixture can be enhanced using the calcined clay with a high content of reactive aluminate. Besides, the presence of uncalcined kaolinite may also affect the structural build-up of fresh LC3 pastes [134].

To date, the implementation of using calcined clay or MK as the cement substitute in 3D printable cementitious materials is still limited. Only a few attempts are available. For instance, small dosages of MK (0–5%) were employed in Refs. [100,135] for modifying the thixotropy of the developed 3D printable cementitious pastes. Bohuchval et al. [136] studied the effects of different proportions of MK (6%, 12%, and 20% of binder mass) on the rheology and printability of fresh mortars. The blend of 24% fly ash and 6% or 12% MK was suggested as an optimal cement replacement for increasing the yield stress and cohesiveness, as well as enhancing printability and reducing water drainage of the developed fresh mixture. Chen et al. [26,101] proposed a series of limestone and calcined clay-based cementitious materials for 3DCP. In their mixtures, up to 60% of OPC was replaced by a blend of limestone and calcined clay in a 1:2 proportion. The impacts of different dosages of VMA on various printability aspects and hardened properties of developed limestone and calcined clay-based cementitious materials were studied in Ref. [26]. In another work [101], the effects of different grade levels of calcined clays on 3D printability, compressive strength, and hydration of such mixtures were investigated. The different calcined clays (containing 50%, 62.5%, and 75% of MK) were made by mixing high grade-calcined clay (HGCC) and low grade-calcined clay (LGCC) in three different proportions. By increasing the HGCC content, the material flow consistency, thixotropy, and buildability were significantly increased; the early-age hydration was slightly accelerated and enhanced, whereas the printability window and interlayer bonding were decreased.

4. Characterization methods of fresh-state and interlayer behaviors

4.1. Fresh properties and test methods

4.1.1. Flowability

The flowability test is a common and straightforward assessment for studying the rheology of fresh cementitious materials. Many conventional methods, e.g., slump and slump flow tests, V-funnel test, and L-box test, show potential to evaluate the flowability of printable mixtures [23,137]. Among them, slump and slump flow tests might be the most appropriate tests to effectively indicate the printability of studied mixtures. Tay et al. [59] mentioned that the slump value (slump test) is dominated by the solid-state physical properties of microstructure and the static yield stress of the printable mixture, which may indicate the buildability in 3DCP. As mentioned earlier, most of the printable cementitious materials from literature belong to mortar technically. Thus, a mini-slump cone with dimensions of 50 mm top diameter, 100 mm base diameter, and 150 mm height [23] for mortar or 19 mm top diameter, 38 mm base diameter, and 57 mm height [138] for cement paste is appropriate to be used for the measurement of slump value. Hägermann cone (70 mm top diameter, 100 mm base diameter, and 60 mm height) was also employed in many earlier studies [26,139,140] to determine the shape retention of fresh cementitious materials. Besides, a cylindrical mold could be applied for the slump test to indicate the buildability of printable cementitious materials (see Ref. [42]). According to Flatt et al. [141], for the very low spread, the yield stress τ_0 of studied mixtures can be obtained using the modified model (Eq (4)) of Murata approach.

$$\tau_0 = \frac{\rho g H}{\sqrt{3}} \quad (4)$$

where ρ is the unit of weight of the mixture, g is the gravity constant, and H is the height of the demolded sample. This model may only be valid once the ratio between the initial height and radius is in the range of 0.8–2.

Hägermann cone is primarily used for performing the slump-flow test (also known as jump table test) of mortar composites. The test procedure could refer to ASTM C1437–15 [142]. The spread diameter is measured to quantify the flowability of studied mixtures and is related to the dynamic yield stress, which may influence the pumpability and extrudability of studied mixtures in 3DCP. Tay et al. [139] found that the fresh mixtures with a slump value within the range of 4–8 mm (Hägermann cone), and a spread diameter between 150 mm and 190 mm showed the optimal printing quality and buildability using their 3DCP setup. In contrast, Ma et al. [23] performed the slump flow test with different material ages and attempted to find the correlation between the flowability and printability window. In their study, the recommended ranges of the slump value and spread diameter for 3DCP were 32–88 mm (mini-slump cone for mortar), and 174–210 mm, respectively. The various findings between different studies may be due to the differences in 3DCP setup and slump cone in the slump test.

4.1.2. Ram extrusion

Ram extruder as a test device commonly comprises four components: a stand frame, a piston, a barrel, and a die with a round or rectangular opening (see Fig. 5 (a)). The fresh mixture is filled in the barrel, and then the ram is driven by a compression device to push the material towards an abruptly constricted or gradually narrowing die [143]. Ram extrusion is used as a tool in the laboratory for investigating the extrusion flow, describing rheological properties, and examining the extrudability of materials [143–146]. As mentioned by Chen et al. [147], ram extrusion can be regarded as an extrusion model for quantifying the fresh properties of printable cementitious materials. Studies from Refs. [50,148] determined the extrudability of their mixtures by measuring the extrusion force. Chen et al. [57] used a ram extruder to measure the extrusion pressure at different material ages to indicate the time-dependent property of extrudability for cementitious materials. Additionally, ram extrusion is also feasible to characterize rheological and tribological behaviors of stiff cementitious materials that cannot be conducted using a rotational rheometer [65,101,143,147,149,150]. The model proposed by Benbow and Bridgwater [151] that employs a plasticity approach is commonly used to analyze the experimental results (extrusion rheology data) from ram extrusion tests. Benbow–Bridgwater equation is expressed as Eq (5) when a sharp-edged orifice equips the ram extruder.

$$P = 2(\sigma_0 + \alpha V^n) \ln\left(\frac{D_0}{D}\right) \quad (5)$$

where P denotes the extrusion pressure. σ_0 is the elongational yield stress, and α and n are the fitting parameters. D_0 and D are the inner diameter of the barrel and die. V is the material flow rate. For studying the ram extrusion rheology of printable cementitious materials, Benbow–Bridgwater model was employed by Refs. [65,72,100,152].

Basterfield et al. [153] pointed out that the fitting parameters α and n in Benbow–Bridgwater equation are non-intrinsic material factors that do not have any physical meaning. The authors have proposed a modified model (Basterfield et al. model, see Eq (6)) that is adapted from the Gibson equation (without the end effect) for characterizing rigid-viscoplastic materials. This model assumes a spherically convergent flow and neglects the shear stress in the barrel. The detailed derivation process was reported by Refs. [150,153].

$$P = 2\sigma_0 \ln \frac{D_0}{D} + \frac{2}{3n} k (\sin \theta_{max} (1 + \cos \theta_{max}))^n \left(1 - \left(\frac{D}{D_0}\right)^{3n}\right) \left(\frac{2V}{D}\right)^n \quad (6)$$

where k and n mean flow consistency and flow index, respectively. θ_{max} denotes the angle of the maximum convergent flow (see Fig. 5 (b)). For most of the paste-like materials, the value of θ_{max} is of the order of 45° (in the range of 40–60°). The obtained elongational yield stress σ_0 can be used to compute the related shear yield stress τ_1 , since the cementitious materials are considered to follow the Von–Mises criterion [146,153].

$$\tau_1 = \frac{\sigma_0}{\sqrt{3}} \quad (7)$$

Zhou et al. [150] investigated the rheological properties of discrete short fiber-reinforced semi-solid cementitious materials by using this model (Eq (6)). Similarly, studies of the authors in Ref. [101] employed Basterfield et al. model to analyze the experimental results of the ram extrusion test for quantifying the effects of different calcined clays on fresh-state behaviors (see the example: Fig. 5 (c) (d)). Based on Basterfield et al. model, Perrot et al. [146] added the contribution of shear stress on the tapered surface and studied the rheological and tribological behaviors of cementitious materials.

Nevertheless, it must be noted that many factors may influence the experimental results of the ram extrusion test. First, the friction between the piston and the inner surface of the barrel is not taken into consideration in many earlier cases. As mentioned by Refs. [57,147], applying silicone release or other types of compounds on the surface of these components is one way to minimize such friction, whereas it is impossible to eliminate this wall friction. Second, a dead/static zone may exist near the die (see Fig. 5 (b)). The test

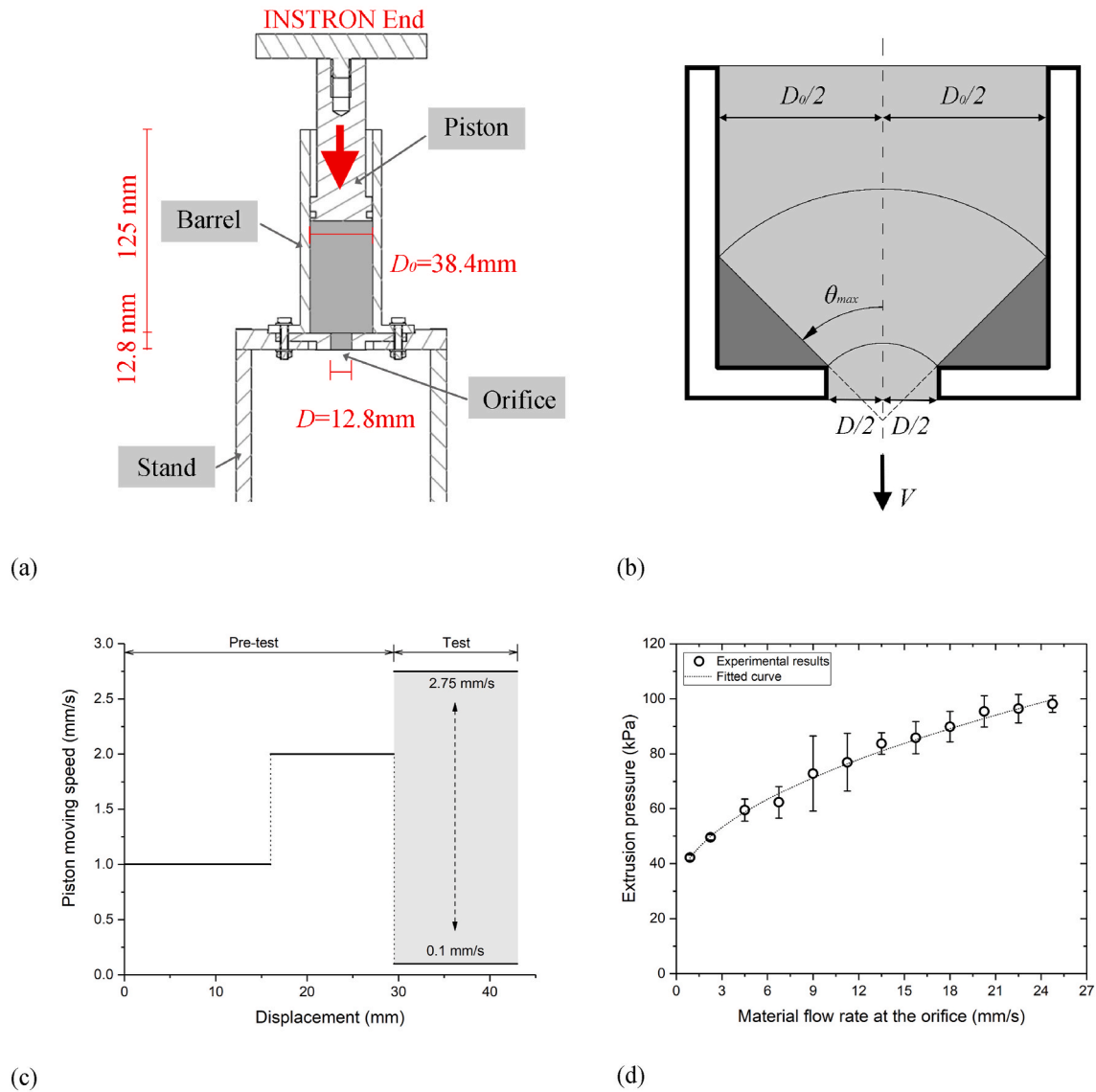


Fig. 5. (a) Scheme of the ram extrusion setup; (b) Illustration of the orifice entrance flow region based on a spherical coordinate system; (c) A predefined ram extrusion test protocol; (d) An example of test results and the fitted curve (Basterfield et al. model). Adapted from Ref. [101].

results from Refs. [50,146,148] revealed that the extrusion force increased irrationally when the piston approached the orifice. Thus, it requires the computation of the maximum length of the dead zone (L_{dz}) via Eq (8) before performing tests.

$$L_{dz} = \frac{(D_0 - D)}{2 \tan \theta_{max}} \tag{8}$$

The maximum value of L_{dz} is obtained when θ_{max} equals 40° . The sufficient distance between the ram and dead zone should be left to minimize the influence of the dead zone, which can be predefined in the experimental program. Third, the fresh cementitious materials are assumed as rigid-viscoplastic materials to be incompressible during the ram extrusion process. The material flow rate V that is not measured directly is calculated by using the predefined ram speed V_0 [150].

4.1.3. Pumpability, extrudability, and open time tests

Pumpability is a primary criterion to assess the fresh properties of some cementitious materials, including self-compacting concrete, shotcrete, and 3D printable cementitious materials. In 3DCP, the term of pumpability is specifically used to indicate the ease with which fresh cementitious materials are delivered from the pump to the printhead (nozzle) [1,24,25]. During the pumping process, problems like the blockage of the hose, extremely high pumping pressure, material bleeding, and particle segregation may be induced by the improper mix designs and pumping rates that are possibly determined using the pumpability test. However, until now,

a standard test protocol and setup for evaluating the pumpability of 3D printable cementitious materials are not available. Many researchers proposed trial-based methods by using their material pumping setups. For instance, Chaves Figueiredo et al. [65] examined the pumpability of different fresh mixtures that showed various shear and bulk yield stresses using a rotor and stator-based pump under the identical pumping rate with or without a hose of 5 m. A similar approach was also occupied by Tay et al. [139].

The pumpability of cementitious materials can be evaluated by the pumping pressure (P) under a specific pumping flow rate (Q) related to Bingham parameters. Eq (9) is used to describe this relation [53,154].

$$P = \left(\frac{8\tau_d}{3R} + \frac{8k}{\pi R^4} Q \right) L \quad (9)$$

where R and L are the radius and length of the hose/pipe, respectively. τ_d and k stand for the dynamic yield stress and plastic viscosity. Since R is commonly smaller than 1 m, τ_d and k dominate the pumping pressure for a specific pumping system under a fixed pumping flow rate. Nevertheless, the quantification of pumpability for printable cementitious materials is still an opened research field. Techniques, like Sliding Pipe Rheometer [155,156] and other visco-/tribo-meters [157], have shown feasibility to characterize the pumpability of ordinary concrete [158]. Further investigation about using these techniques for quantifying the pumpability of printable cementitious materials is urgently needed.

Extrudability is used to describe the ability to continuously print the material through a (round or rectangle opening) nozzle with an acceptable printing quality (minimum degree of tearing/splitting of extruded filament) [1,25,51,159]. The extrudability test in this study means the inline measurement of the extrudability of 3D printable cementitious materials by using a 3DCP setup as an experimental device. Most of the extrudability measurements belong to the qualitative characterization [3]. Visual inspections have been applied to evaluate the printing quality of deposited filaments, i.e., surface quality and dimensional consistency. Kazemian et al. [51] stated their evaluation criteria of printing quality: (1) no surface defects, (2) visible layer edge, (3) dimension conformity. The authors measured the width of the single printed filament at different positions for checking the printing consistency. Similar approaches were adopted in Refs. [73,75,160]. As mentioned by Refs. [26,45,50], the filament dimension consistency depends on not only the fresh-state behaviors of materials but also the relation between the linear flow rate of material (V_m) and nozzle moving speed (V_n). If $V_m > V_n$, the 'buckled' layer could be observed. In contrast, if $V_m < V_n$, it could result in width reduction or even discontinuity of the extruded filament. Generally, V_m should be equal to V_n during the printing process. Additionally, Nerella et al. [50] introduced an inline and quantitative method for characterizing the extrudability of 3D printable cementitious materials. Under a specific material flow rate, the required energy (electric power) for extruding the fresh mixture was measured and recorded as the corresponding extrudability index-unit extrusion energy (UEE) [J/cm³]. For achieving a similar printing quality, the material with a smaller value of UEE is more extrudable.

Due to cement hydration, yield stress increases with time. Pumping and extrusion operation windows should be determined to ensure acceptable printing quality and to avoid nozzle blockage [1,24,161]. Open time, also known as the printability window, is defined as the operation window for extrusion of a given volume (batch) of printable cementitious materials. It is to be noted that the open time is only significant for the printing process with multiple batches of material preparation. The volume of each batch is relatively large, such as 45–60 L, and the required time for completely extruding one batch of material is 30–60 min (material flow rate: 1–1.5 L/min). In this case, only the printable material with a minimum open time of 30 min is allowed. Inline measurement of open time was proposed by studies [23,26,101]. At a predefined printing speed, a filament with the designed dimension is extruded from the 3DCP setup at different material ages. The width of the filament is measured at different positions to evaluate the dimensional consistency of printing. The time gap between the two subsequent filaments is 10 min. During the time gap, a pre-shearing process is required due to the thixotropic nature of the cementitious material. The test is terminated once the filament disruption occurred, or the width of filament becomes 10% smaller than the design width. The test time is referred to the open time of the tested material (see Fig. 6). Moreover, applying offline approaches at different resting times, including slump and slump flow tests [26], shear strength measurement [25], and ram extrusion test [57], show great potential for indicating the open time of printable cementitious material. Most of these tests have attempt to characterize the workability loss of fresh cementitious material with time.

4.1.4. Buildability

Buildability is used to indicate the shape retention property of deposited material under the gradually increasing load induced by the subsequent upper layers [24]. Generally, the buildability is characterized as the maximum layer number that could be built up by using a fresh mixture [25,101,139]. In many cases, the height of the deposited layers is measured to quantify the material plastic deformation to evaluate buildability [23,26,51,88]. It must be noted that the printing parameters, i.e., the geometry and length of printing/nozzle path (shape of the designed object for printing), nozzle variables (shape, dimension, and flow direction), the time intervals between two subsequent layers (also known as cycle time [1]), nozzle standoff distances and printing speeds, may significantly influence the buildability assessment.

Extending the time gap between successive layers could improve the buildability of printable cementitious material since the stiffness and rigidity of the deposited layer develop with time, which is related to the flocculation and nucleation between cement particles at rest [28]. For a non-stop test process, the time interval is primarily dependent on the printing path length and printing speed [26]. As mentioned by Wolfs et al. [162], two failure modes can be observed during the buildability test: material plastic collapse and elastic buckling failure. Material failure is induced by the exceeded load on the deposited layer, leading to yielding and flow out. In contrast, the local or global instability of layered structure can result in the uncontrolled deformation [2,162]. The former one appears to be mainly dominated by the static yield stress/green strength of printable cementitious material. The resistance of material

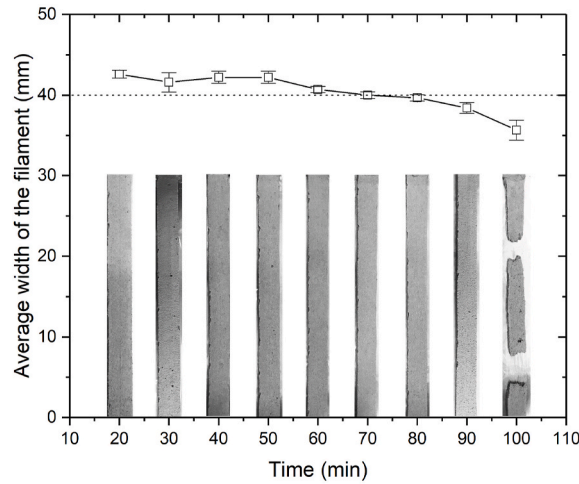


Fig. 6. An example of the open time measurement. The width of the nozzle opening used in this test is 40 mm.

failure can be improved by enhancing and accelerating the yield stress development of deposited materials at rest [31]. From the material perspective, a possible solution is to reach setting by accelerating very early-age hydration via physical and/or chemical approaches (see Refs. [31–33]). However, elastic buckling failure can be attributed to material behavior and process variations. Most local instability may occur induced by the changes in boundary and geometry conditions during the printing process [2,27,162,163]. The geometry of the printing path is critical in this context. For instance, printing a straight and long wall may fail relatively easily compared to a curved wall with the same path length because the curvature of the wall would likely increase the structural stability [2].

Another critical stability issue concerns the nozzles with a down-flow direction and round opening, where a new layer compresses the substrate layer upon deposition. Here, the bottom layer needs to sustain a combination of the load from the weight of the new layer and the force applied by the nozzle [101,164]. Due to the deformation of substrate layers, this load may be decreased by adjusting the nozzle standoff distance that also recovers layer thickness (see Fig. 7 (a)). Once the load reaches the yield stress of the substrate, material collapse is expected. However, buckling failure induced by a high nozzle standoff distance may occur before material

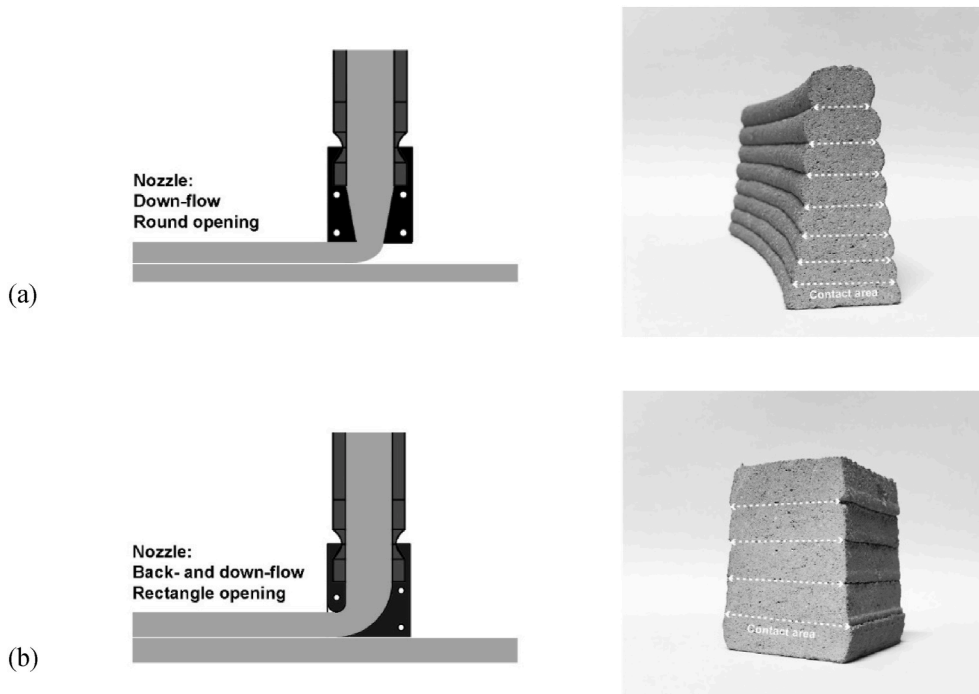


Fig. 7. (a) Illustration of the printing using the down-flow nozzle with a round opening and the cross-section of the printed sample. (b) Illustration of the printing using the back- and down-flow nozzle with a rectangle opening and the cross-section of the printed sample. The dashed line represents the contact area between layers. Modified from Ref. [101].

failure (see Fig. 8 (a)). Misalignment of the printing path and a dropped layer process can reduce the contact area between two subsequent layers, increasing the possibility of buckling collapse [4,5]. Employing a back-flow or hybrid back- and down-flow nozzle with a rectangle opening can increase the contact area between two layers resulting in a more stable printing process [27] (see Fig. 7 (b)). Nerella et al. [165] used a back-flow nozzle with a rectangle opening to print a straight wall for assessing the resistance of material failure. A similar approach was performed by Chen et al. [101]. It is noteworthy that the excess material on both sides of each filament must be appropriately removed (the printer could not be terminated after finishing one filament immediately). Uncontrolled shapes and positions of the filament boundaries/sides could result in a severely buckling collapse. As introduced by Mechtcherine et al. [3], an advanced printhead containing a shutter that could automatically stop the printing for finishing the filament is a solution to improve this buildability test (see Fig. 1 (d)). Furthermore, many other studies [23,88,162,163] used a different method to perform a straight wall printing test. They employed a down-flow nozzle with a rectangle opening, and the wall was printed in a continuous printing trial. As shown in Fig. 8 (b), this process may lead to more material deposited on both sides (start and end printing points) than other regions of each layer. The excess deposited material on both sides potentially influenced the stability of the printed structure, which may be the reason for the elastic buckling failure initiating from one side in Ref. [162].

In the buildability test, local instability of a printed structure can cause stress concentrations resulting in material failure. In many cases, it is hard to determine the dominant source of test failure. Process monitoring techniques appear to be very useful for a better inspection and understanding of the failure during the buildability test [165]. The gradually increased layer deformation can be measured using optical sensors [148] or analyzing the images recorded during the test process [166].

4.1.5. Green strength

Since it can take up to 3–4 h to print one building component (about 3 h is required to print a wall with 3 m height at the building rates of 1.1 m/h from Ref. [167]), the yield stress evolution of the bottom layers is severely critical during this period. Applying direct load on the fresh cementitious materials is one way to determine the applicable building rate and to assess shape stability for specific printable materials [31,167]. Perrot et al. [167] simulated the loading induced by the layer-by-layer construction process on the first deposited layer by using a plate-stacking test. The cylindrical sample with a 60 mm diameter and 30 mm height (aspect ratio: Height/Width = 0.5) was employed and placed between two parallel plates. The authors applied a 1.5 kN load increment on the top plate with a time gap ranging from 11 s to 60 s, simulating a building rate of about 1.1–6 m/h. The deformation of the tested sample was recorded using an LVDT-type displacement transducer. Similar approaches can be found in studies [7,27,51,140,168].

Measuring the uniaxial unconfined compressive strength of fresh cementitious materials at different ages (e.g., within the first 4 h) is an approach to monitor the very early-age strength development of studied mixtures. The obtained compressive strength can be regarded as the green strength of the tested young age sample [169]. In such a test, cylindrical samples with an aspect ratio of 2 are commonly used [26,55,57,166,169–172]. This aspect ratio can indicate the failure of printed structure [31] and also allows the formation of a diagonal shear failure plane [166]. Displacement control at a rate of 0.2–0.5 mm/s [26,57,166,170,172] is usually preferred for performing the green strength test. Up to 20–25% of strain could be reached for each sample eventually. Note that, as mentioned by Refs. [26,166], a double-layer of Teflon or other types of sheets should be placed on both sides of the sample to reduce friction between sample and steel base plates. Optic measurement methods (see Refs. [26,55,57,166,172]) should be employed to record the horizontal displacement of the sample during the test. According to the test results in most studies [55,57,166,170,172], two typical strain/stress curves and crack patterns can be observed (see Fig. 9). For the samples with younger ages (within the first 1 h, how-

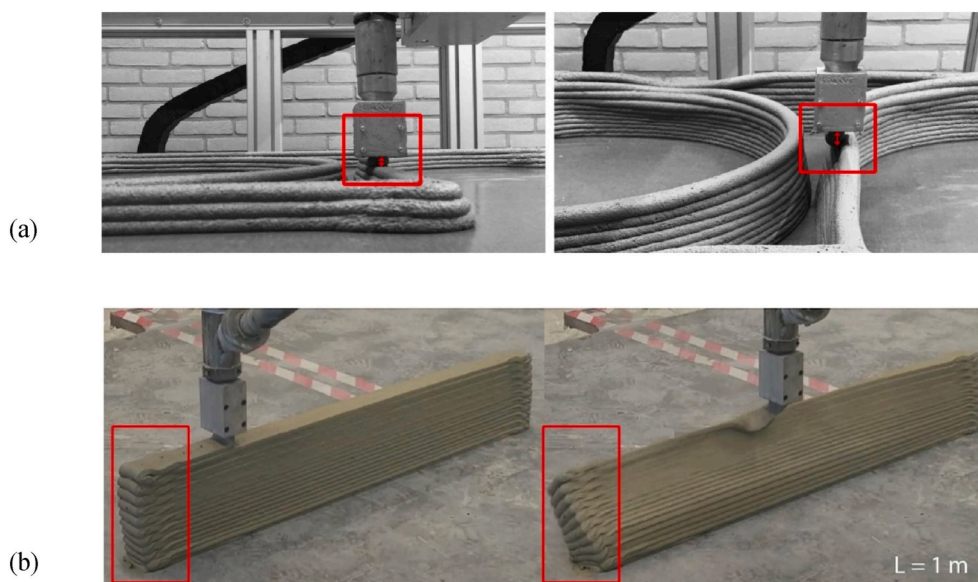


Fig. 8. (a) Printing failure induced by the increase of nozzle standoff distance, adapted from Ref. [101]; (b) The excess material deposited on both sides of each filament, adapted from Ref. [162].

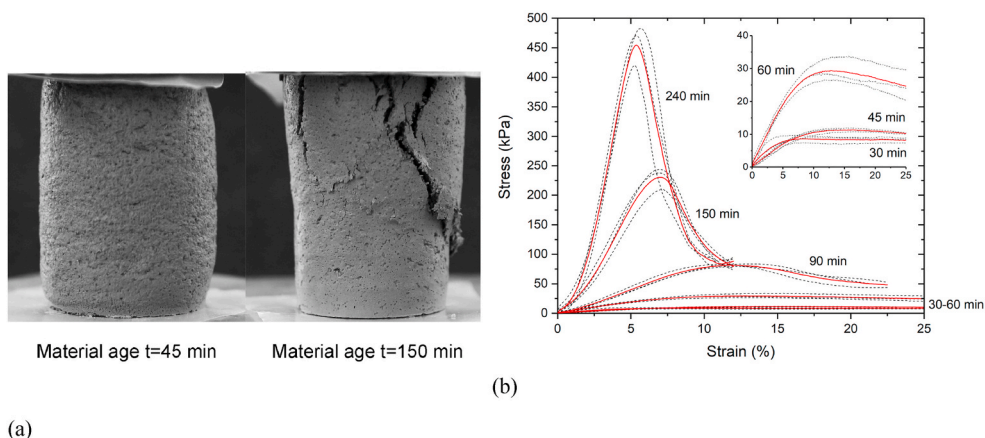


Fig. 9. (a) Typical failures observed in green strength tests at different material ages; (b) Typical stress-strain relations in green strength tests. Modified from Ref. [57]. (For interpretation of the references to colour in this figure legend, the reader is referred to the Web version of this article.)

ever, it largely depends on the mixture), the stress near-linearly increases with the increase of strain until to reach a plateau. The cross-section of the sample expands during the increase of deformation. Finally, instead of forming a distinct crack pattern, the young age sample fails with a barreling effect. In contrast, for the samples with older ages (after 1 or 2 h), a strain-softening behavior is observed after the stress reached the peak value. Meanwhile, more distinct cracks are formed during testing of older age samples. Additionally, the obtained experimental results could be used as one of the inputs for optimizing the printing process via numerical studies (see Refs. [162,166]). The shear strength of fresh cementitious materials at different ages can be conducted by using direct shear tests. More details about direct shear tests can refer to studies [166,173].

4.1.6. Penetration resistance

The penetration test is a continuous mechanical measurement to indicate the structuration of fresh cementitious materials at rest [174]. The penetration setup is very commonly used in the field of civil engineering, e.g., Hilti nail gun, Vicat, and Gillmore needles [175], penetration plunger [176], and penetrometer [177]. In the cases of Vicat needle and cone plunger tests, the penetration force is kept identical (induced by the weight of the needle or plunger), and the penetration depth is used to indicate the stiffness of fresh cementitious materials [175,176]. The use of a Vicat needle to investigate the setting behavior of 3D printable cementitious materials could be found in Refs. [57,72,178–182]. During the Vicat test, two forces induced by the tested materials, i.e., compressive and shear resistances, are exerted on the needle. A balance between the Vicat needle's gravity and such resistances could be reached during the initial and final set of cementitious material [183]. If assuming a plastic failure criterion for the compressive resistance in this context, the compressive strength is of the order of twice the shear strength [183,184]. The force equilibrium equation can be expressed as:

$$\tau_p = \frac{mg}{2\pi rh + 2\pi r^2} \quad (10)$$

where τ_p is the shear strength, and h is the penetration depth. m and r denote the mass and radius of the Vicat needle. However, due to the standard dimension of cone mold and penetration needle, the Vicat apparatus can only measure or indicate a limited range of static yield stress, especially between the initial and final setting times of the studied mixture. This could not satisfy the demands for monitoring the yield stress evolution of printable cementitious material at a very early age (for example, after depositing the first several layers).

Penetrometer uses a different technique in comparison with Vicat. The penetration tip is driven at a constant speed to penetrate the sample, and the required force is measured and recorded at different material ages until the final set [177]. Customized penetrometers were developed and employed by researchers [175,185,186]. The penetration resistance measurement based on a penetrometer could be used to determine the stiffness development of fresh printable cementitious materials directly, see Refs. [23,51,187]. Compared to the Vicat test, the penetration test performed by using a penetrometer could measure a broader range of yield stresses from 1 kPa to 200 kPa, which is of interest for indicating the structuration of the deposited material in digital fabrication of concrete [174]. Lootens et al. [177] employed many penetration tips with different geometries (conical and hemispherical) and dimensions (see Fig. 10) in the penetration test under a slow speed (1 $\mu\text{m/s}$). The relations between the yield stress of the cement paste and penetration force in different conditions were determined in their work (see Table 2). The penetration forces scale with the yield stress, which is related to the contact surface between the penetration tip and tested materials. It should be noted that the yield stress in their study was obtained from ultrasonic measurements. Different contact surfaces could be attributed to the different shapes and sizes of penetration tips. The correlation between penetration forces and yield stress in Ref. [177] was validated and strengthened by Ref. [173]. The authors studied the very early-age strength development of self-compacting mortar that was employed in slip-forming by employing a set of mechanical experiments, including compression (green strength measurement), tensile, shear, and bending tests. Similar validation can be found in Refs. [32,174]. Based on these studies [32,173,174,177], using penetration measurement could in-

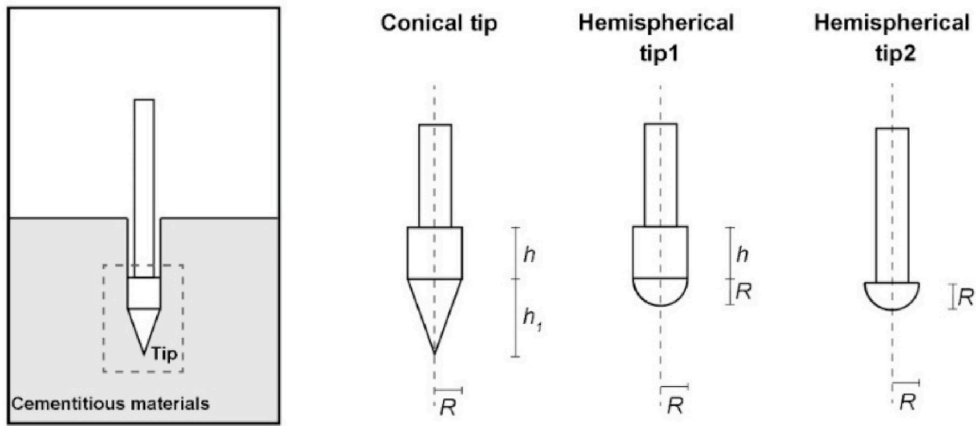


Fig. 10. Schematic illustration of different penetrometer tips, modified from Ref. [177].

Table 2

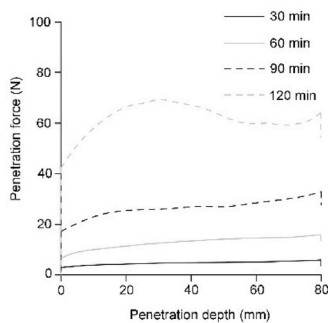
A summary of relations between penetration force (obtained by penetrometer measurement) and yield stress (from Lootens et al. [177]).

Penetrometer type	Parameter	Relation with yield stress or compressive strength (or green strength)
Conical tip	Radius R , Cone height h_1 , and connected cylinder height h	$\tau_0 = \frac{F}{\pi R \sqrt{R^2 + h_1^2} + 2\pi Rh}$
Hemispherical tip1	Radius R , and connected cylinder height h	$\tau_0 = \frac{F}{3\pi R^2 + 2\pi Rh}$
Hemispherical tip2	Radius R	$\tau_0 = \frac{F}{3\pi R^2}$

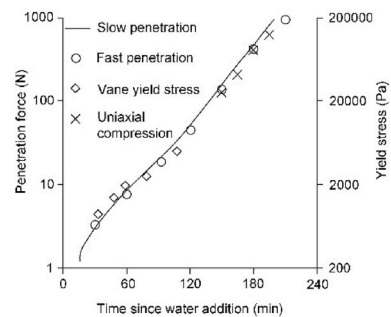
* F stands for the measured penetration force.

dicating the yield stress evolution of fresh paste and mortar, which showed good agreement with the results obtained by compression, vane rheometry, ultrasound, and other tests (see Fig. 11 (b)).

In comparison with slow penetration measurement in Ref. [177], the fast penetration test (see Fig. 11 (a)) has also been applied by many studies [173,174,188] (penetrating rate: 1 mm/s). As shown in Fig. 11 (b), similar results can be obtained at either fast or slow rates [174]. However, in the fast penetration test, multiple samples are required for determining the yield stress at different rest times. Compared to the fast one, the slow penetration test can provide a continuous measurement of yield stress for the tested materials using a single sample. This advantage becomes quite significant if an extended period test is of interest [32,174]. Nevertheless, the limitations of the penetration test should be noted. Reiter et al. [32] stated that the yield stress in mortar and concrete is dominated by friction between aggregates, which is also variable with time induced by water consumption of cement hydration process. The internal friction angle cannot be determined via penetration measurements directly. The slow penetration test currently has only been applied to examine the yield stress of mortar that contains a small volume fraction of sand.



(a)



(b)

Fig. 11. (a) Fast penetration test at different times (using conical tip); (b) The evolution of penetration force and yield stress obtained by using different approaches. Both (a) and (b) adapted from [174].

4.1.7. Rheometry

The coaxial rheometer has been successfully used to characterize the rheological behaviors of 3D printable cementitious materials in many earlier studies [42,44,47,48,52,53,84,189]. The vane-in-cup geometry is very suitable and commonly used to study the rheology of concentrated suspensions [190,191]. Some 3D printable cementitious materials containing fine aggregate (maximum size: 1 mm) can be tested by using this geometry [1]. The employment of rheometry with different specific test protocols could characterize the minimum shear stress, critical strain for flow, suitable printing rate (material flow rate) for extrusion, and the structural build-up of cementitious materials after deposition [189,192].

(1) Flow onset

Due to the thixotropy, the rheological behavior of fresh cementitious materials largely depends on their flow history. Therefore, care should be taken before starting the measurement of the shear stress peak and critical strain for ensuring the test reproducibility. It is essential to perform a pre-shearing process to keep the same destructed status [192,193]. A specific protocol of the constant shear rate (CSR) test proposed by Roussel et al. [194] was recommended and summarized. First, during the pre-shearing session, the sample is sheared at a relatively high shear rate (e.g., 150 s^{-1}) for about 200 s. Second, the sample is kept at rest of 5 min and afterwards tested under a constant and low shear rate (e.g., 0.005 s^{-1}). Consequently, a typical shear stress VS. shear rate curve can be obtained in Fig. 12 (a). It could be found that the shear stress showed a linear increase before it reached the yield stress. This demonstrates the elastic behavior of tested material in its solid regime. The material starts to flow after the shear stress and strain exceeds the static yield stress and critical strain. The peak stress is related to the breakage of attractive colloidal interactions between particles. Besides, as shown in Fig. 12 (b), another peak stress can be identified before the critical strain because of the breakage of hydrates formed between particle grains [192].

(2) Hysteresis loop test

Fresh concrete can be described as a Bingham fluid within a specific range of shear rates. For a typical Bingham material, the shear stress, above the threshold value for flow called yield stress, is increased linearly with the increase of shear rate [195]. The Bingham model is expressed as Eq (11).

$$\tau = \tau_d + \mu_p \gamma \quad (11)$$

where τ and γ are the shear stress and shear rate. τ_d and μ_p denote the yield stress and plastic viscosity of the tested material. In many studies [7,47,53,54,135,140,196,197], 3D printable cementitious materials were assumed to show the Bingham fluid behaviors within a range of shear rate. A hysteresis loop test protocol can be employed by using the rheometer in this context. As shown in Fig. 13 (a), the shear rate was increased from 0 s^{-1} to the maximum value (e.g., 60 s^{-1} , 100 s^{-1} , or 200 s^{-1}) within a short time. The shear rate was directly decreased to 0 s^{-1} at the same time as it increased (see Refs. [53,54,135,196,197]), or it was kept at the maximum value for about several minutes and then decreased to 0 s^{-1} (see Refs. [7,47,140,189]). The relation between the measured torque/shear stress and shear rate showed a thixotropic loop containing the up and down curves (see Fig. 13 (b)). The larger the enclosed area between the up and down curves, the higher the thixotropy of the tested material [196]. The down curve could be used to fit Bingham model (Eq (8)) for obtaining the flow parameters, including dynamic yield stress and apparent viscosity [47,53,196]. These material parameters can be used to compare different mixtures and achieve the optimal mix design of 3D printing. According to Refs. [26,158], the fresh mixtures should exhibit moderate dynamic yield stress and relatively low apparent viscosity for displaying favorable pumpability and extrudability. Additionally, based on the test results of hysteresis loop measurement, Herschel-Bulkley model was found to be more suitable for characterizing the dynamic rheological behaviors of some 3D printable cementitious materials, and more details could refer to Ref. [135].

Nonetheless, it must be noted that the wall slip phenomena cannot be avoided in rheometry, no matter what the applied rotor geometry is used [1,191], mainly when we test the printable mixture with high stiffness and less fluidity. Once the material contains

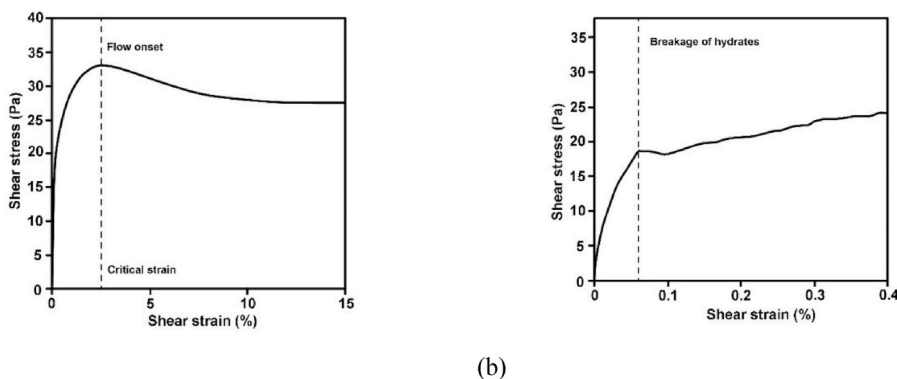


Fig. 12. CSR test of cement paste (W/C = 0.4)-the relationship between shear strain and shear stress. (a) Shear strain from 0% to 15%; (b) Shear strain from 0% to 0.4%. Adapted from [194].

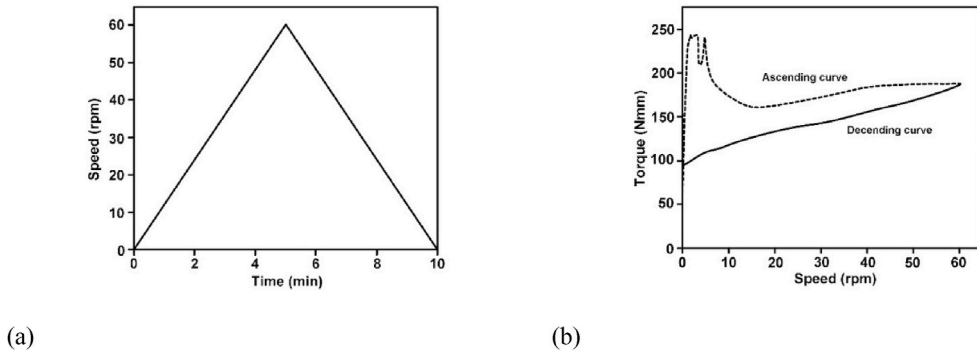


Fig. 13. (a) A hysteresis loop test protocol; (b) A typical result of the hysteresis loop test. Adapted from Ref. [53].

aggregate, even fine sand (less than 1 mm of diameter), particle migration can occur during the measurement, leading to the measured viscosity lower than the expected one [1]. Besides, for the same material (at the same material age), the results of Bingham fluid parameters obtained by using different rheometers and/or test protocols seem to be less comparable, probably due to the variables in flow history.

(3) Structural build-up

For quantifying the structuration rate of fresh cementitious materials at rest, two methods are commonly employed, including the CSR test and small amplitude oscillatory shear (SAOS) test [198]. Both methods have been applied in the context of 3D printable cementitious materials. In this case, the CSR test can be performed at different material ages for determining the evolution of material static yield stress. The obtained static yield stresses at different ages could be furtherly used to predict the structuration rate of the studied material [167,198–201]. Due to the low yield stress of self-compacting concrete, a very low shear rate, such as in the range of $0.001\text{--}0.01\text{ s}^{-1}$ [194,201–203], is feasible to reach flow onset within a short test duration (e.g., 100–200 s) [189]. In contrast, the printable cementitious materials show relatively high stiffness. Also, this test is conducted at different material ages. With time passing, the rigidity and stiffness of studied fresh cementitious material are increased. According to Yuan et al. [203], a relatively long test duration is required for achieving flow onset by using the slow shear rate ($0.001\text{--}0.01\text{ s}^{-1}$), which may not be suitable in this situation. Nerella et al. [189] introduced a strain-based test method for quantifying structural build-up of printable cementitious materials. They employed different shear rates from 0.08 s^{-1} to 0.24 s^{-1} at different resting times. A similar approach was used in Refs. [132,134]. Their results confirmed that the structuration of less/non-flowable cementitious materials could be characterized via this strain-based approach.

The measured static yield stresses at the different material ages could be analyzed by using either the linear model (Eq (12)) proposed by Roussel [82] or the exponential model (Eq (13)) from Perrot et al. [167].

$$\tau(t) = \tau_{0,0} + A_{thix}t \quad (12)$$

where $\tau_{0,0}$ and A_{thix} mean the initial static yield stress and structuration rate constant that is the increased rate of static yield stress over time. The exponential model is the extension of the linear one since the structural build-up of cement paste showed an exponential increase after a critical time point (t_c), as reported by Perrot et al. [167].

$$\tau(t_{rest}) = \tau_{0,0} + A_{thix} (e^{t_{rest}/t_c} - 1) t_c \quad (13)$$

The value of t_c is used to adjust the curve to achieve the best fit with test results. When t_c tends to 0, Perrot et al. model asymptotically tends to Roussel model. According to Refs. [2,167], the value of t_c is related to the setting of the studied material.

SAOS test is a proper way to investigate the viscoelastic properties of fresh cementitious materials for studying the structuration behavior [189,192,204]. Both static yield stress (CSR test) and elasticity (SAOS test) are essential for evaluating the structural build-up of printable cementitious materials since both colloidal and hydration effects strongly influence the control of the printing process, e.g., shape retention for each layer, building rate, and stability of printed structure [192]. The SAOS test procedures can be described as: applied a continuous sinusoidal excitation with a controlled shear strain (deformation) on a single sample and recorded the stress response [189,192,198,204]. The complex modulus (G^*) can be given as Eq (14).

$$G^* = G' + G''i \quad (14)$$

G' is the storage modulus that belongs to the in-phase and elastic component of the response. In contrast, G'' means the loss modulus, and is the out-of-phase and viscous component of the response [192]. The SAOS test can be regarded as a nondestructive approach, when a very low excitation is applied, which could ensure the tested material remains in the elastic regime [204]. For cementitious pastes, the applied strain is 10^{-4} to 10^{-5} (with or without superplasticizer), which is also the critical strain range of such materials [198,204]. The evolution of G' with time showed a similar pattern with static yield stress obtained using a CSR test

[189,203]. As mentioned earlier, the critical strain of cementitious materials in the SAOS test is related to the breakage of C–S–H bridges between cement particles [189,192,194]. A few examples employed the SAOS test for quantifying the viscoelastic properties of 3D printable cementitious materials. Tay et al. [44] measured storage modulus G' development of studied material over time. They found that the storage modulus at the bottom layer strongly influenced not only the layer stability but also the interlayer bond strength. Moeini et al. [205] studied the effects of superplasticizer and nano-clay on the critical shear strain and storage modulus of their pastes at different resting times. However, as mentioned by Refs. [2,198], the SAOS test is only valid for pastes and fine mortars. Sensitive and expensive devices are required.

On the other hand, a large amplitude oscillatory shear (LAOS) test is a promising method to characterize the thixotropy of cementitious materials [1,192,206]. As stated by Conte and Chaouche [206], the yield stress and flow curves measured by using the SAOS test cannot be defined rigorously in cementitious materials, since the test duration and flow history dominate such properties. The steady-state cannot be reached under a stress or strain rate in the SAOS test of cement pastes. Theoretically, the flow curve cannot be obtained in this case. Compared to the SAOS test, the LAOS test showed many advantages for dealing with non-linear properties, such as thixotropy, shear-thinning, or -thickening. Generally, the rheometer equipped with a cross-hatched parallel plate geometry was employed for performing the LAOS test [1,131,206]. An example of using the LAOS test to study the flow behaviors and predict the open time of 3D printable cementitious materials was reported by Ref. [1]. Further study is still required to provide more data and details of such tests.

4.2. Interlayer behaviors and test methods

Compared to mold-cast cementitious materials, interlayer behaviors may be the most critical research direction for 3D printed cementitious materials. Thus, hardened properties and test methods related to the interlayer behaviors of 3D printed cementitious materials were discussed in detail.

4.2.1. Interlayer bonding

Due to the layer-by-layer printing process in 3DCP, the interlayer bonding, also known as interface, and layer adhesion, is a potential and unavoidable weak point in the 3D printed structure [167,207,208]. The weak interlayer bonding that is also referred to 'cold-joint' could result in anisotropy and affect both mechanical performance and durability of the printed element/structure [207,209]. As mentioned earlier, the high thixotropy/structural build-up of printable material is desired. However, a weak interface may be formed because of the high thixotropy [28,101,210–212]. Except for the thixotropy, many printing parameters may also influence the interlayer bond strength.

4.2.1.1. Printing parameters. According to Refs. [4,5,44,213], different printing parameters might affect the interlayer bonding of the printed cementitious material. In this study, the following parameters that have been reported in earlier works were selected and discussed.

(1) Time intervals

The time interval between two subsequent layers may be one of the most critical printing parameters influencing both buildability and interlayer bond strength. By extending the time gap between layers, the shape stability of deposited layers could be enhanced [26,167], whereas the interlayer bond strength may be significantly reduced [4,5,44,213]. In literature, the time interval ranges from several seconds/minutes to more than 24 h. For the short time intervals (within 1 h), the structural build-up behavior of deposited materials has a severe impact on the layer adhesion. Tay et al. [44] reported a good correlation between the interlayer bond strength and the storage modulus evolution of material over a series of short time intervals (1–20 min). Wangler et al. [161] pointed out that the maximum operation time (time gap) $t_{h,max}$ for avoiding the cold-joint is primarily dependent on the structuration rate A_{thix} and plastic viscosity μ_p of printable cementitious materials (see Eq (15)), for the fixed printing parameters, such as speed, nozzle standoff distance and others.

$$t_{h,max} = \frac{\sqrt{\frac{(\rho gh)^2}{12} + \left(\frac{2\mu_p V}{h}\right)^2}}{A_{thix}} \quad (15)$$

where ρ , g and h denote the density of the material, gravity constant, and layer thickness. V is the printing rate in the horizontal direction.

For some printable cementitious materials, increasing the time interval between layers could increase the chance of air void formation at the interface region [5,44,56], which can be regarded as the main reason for reduction of the interlayer bond strength. The formation of the air void seems to be mostly dependent on the stiffness of the bottom layer. For a relatively long-time gap (tens of minutes but within an hour), the deformation of the substrate after depositing the top layer is reduced due to the evolution of material stiffness that may be attributed to the material drying process and nucleation between cement particles. Consequently, fewer efficiently interacted bond areas between layers are formed, and many unfilled areas are left, resulting in wide macropores/air voids at the interface [5], as illustrated in Fig. 14. However, after long-time intervals, such as a few hours, or even tens of hours, the printing environment may dominate the interlayer bond strength instead of the thixotropy of material since the deposited material may be set already.

(2) Printing environment and curing condition

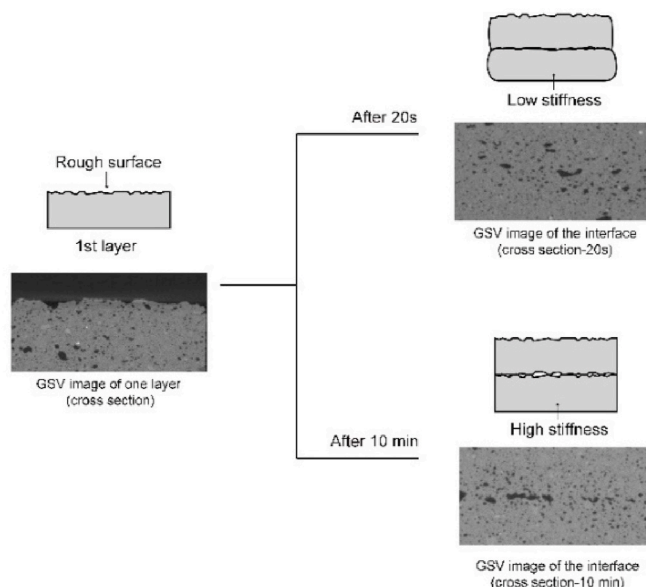


Fig. 14. Illustration of air void formation induced by extending the time gap between layers, adapted from Ref. [5].

In practice, it may require several printing sessions to finish a large-scale building element. The time gap between two sessions can range from several hours to one day that is regarded as the long-time interval. The impacts of the printing environment on interlayer bonding may become significant [5]. Many studies [4,213,214] attempted to investigate the effect of long time-intervals on the bond strength of printed samples. For example, Panda et al. [213] measured the bond strength of printed samples with up to 6 h of time gap. Wolfs et al. [4] extended the maximum time interval to 24 h. If keeping the time gap identical, the curing conditions of the first/deposited layer(s), including the ambient temperature, and humidity, may dominate the interlayer bonding of printed samples. Both the ambient temperature and humidity could influence the drying rate of deposited materials. As reported by Refs. [28,210], exposing the substrate under the drying environment can induce a severe reduction of bond strength. Keita et al. [210] pointed out that the superficial, extremely localized drying is attributed to the origin of this decrease in interlayer bond strength. In contrast, protecting the layer from drying during the time interval, such as increasing the moisture of the deposited layer, is a proper way to improve the layer adhesion. A good correlation between the moisture content and interlayer bond strength was observed by Refs. [182,215].

(3) Nozzle standoff distances

The deformation of deposited layers is unavoidable, and it is hard to keep the default setting of nozzle standoff distance continuously during the printing process. The nozzle standoff distance is increased with the growth of substrate deformation. The increase of nozzle standoff distance increases the possibility of inaccurate layer deposition, changing the contact areas and pressures between layers. Therefore, the interlayer bonding may be influenced [5]. The effects of different nozzle standoff distances on the interlayer bonding have been studied by Refs. [4,5,213]. By increasing the nozzle standoff distance, a severe reduction in more than 30% of bond strength was reported by Panda et al. [213]. In contrast, Wolfs et al. [4] and Chen et al. [5] found less significant effects of this parameter on the average interlayer bond strength. Only the standard deviations of results were increased by increasing the nozzle height from the default value in their studies. The various effects between different studies may be attributed to the variables of materials and printing setup, especially the nozzle types.

(4) Nozzle types

The nozzle variables include the flow direction (e.g., the down-flow, back-flow, or hybrid of back- and down-flow), the size and geometry of the nozzle opening (e.g., round or rectangle). The down-flow nozzle (for both round and rectangle openings) may enhance the interlayer bond strength of the printed sample, mostly when the nozzle standoff distance is smaller than the width or diameter of the nozzle opening. This is due to the fact that the nozzle may add extra force on the deposited substrate. The pressing layer process may provide good compaction and increase the contacted areas between two layers. This pressing force should be diminished with the increase of nozzle standoff distance induced by the layer deformation. Once the nozzle standoff distance is equal to the width or diameter of the nozzle opening, the effect of the down-flow nozzle on interlayer bond strength is minimized, which is the same as the back-flow nozzle. In this situation, the substrate only sustains the gravity-induced dead weight of the top layer. The hybrid of back- and down-flow nozzle (generally with a rectangle opening) may be a better choice to compare with totally down-flow or back-flow nozzles [27]. The material flow angle in the hybrid-flow nozzle can be adjusted/designed by the researchers for providing suitable pressing force, which is less than that of the down-flow nozzle but is still sufficient for increasing the contact areas between layers. However, to date, the optimal nozzle for 3DCP is still an opened research question. It requires a series of tests to validate how these variables influence bond strength and printability quantitatively.

4.2.1.2. Measurement of interlayer bond strength. Experimental approaches, i.e., uniaxial tensile, splitting, and flexural tests, are generally conducted by researchers to quantify the interlayer bond strength of the printed sample. As a direct way to obtain the bond strength, uniaxial tensile test was utilized by many studies [5,44,99,182,213–216]. For tensile splitting and flexural tests, the readers could refer to Refs. [4,207,212,214,217]. However, due to a lack of standard, variable test parameters, including sample sizes, boundary conditions, loading rates, and setups, were adopted in different papers and yielded many difficulties in comparing the results. The same issues can also be observed in tensile splitting and flexural tests. In most cases, the test results obtained from different studies are incomparable. For example, two types of boundary conditions for the uniaxial tensile test were implemented in literature: rotating and non-rotating loading platens (see Fig. 15). Wolfs [27] performed uniaxial tensile tests of printed samples under both boundary conditions for comparing the differences. In his results, both pre- and post-peak can be achieved by using the non-rotating loading platen, whereas only the pre-peak was rational and can represent the tensile behavior of specimen by using the rotating loading platen. Besides, the measured tensile strength (peak load/cross-section of the sample) via uniaxial tensile test with rotating loading platen was slightly lower than the obtained value in non-rotating condition. Due to the rotating supports, uneven deformation occurred during the whole test, which was less evident in the case of non-rotating platen. This uneven deformation appeared to be enhanced by increasing the degree of rotation. Compressions showed negative values in the load/displacement curve were expected at a very early test point and became pronounced since the cracking initiates. Consequently, the rotating condition may induce a bending moment, which led to the extra stress concentration at the beginning of the test [27]. Even using the non-rotating loading platen can show the required material behaviors regarding fracture mechanics, the current set-up of uniaxial tensile test in Refs. [5,27] is still not the ideal one. Limited by the small sample size, the deformation was measured in between the two steel plates (see Fig. 15) instead on the sample locally. Increasing the sample size by increasing layer thickness or casting excess materials on both sides [148,218] may properly address this issue.

4.2.1.3. Methods for enhancing the interlayer bonding. Other than applying the suitable printing parameters during the printing process, two main techniques were employed in the literature for improving interlayer bond strength between layers of the printed cementitious materials.

(1) Increasing the contact area between layers

A lack of effective contact areas between layers is a critical issue resulting in the high void content at the interface. For increasing the effective contact areas, Zareyan and Khoshnevis [212] made interlocking between two subsequent layers, which indicated clearly enhancement of interlayer bond strength. Similarly, Van der Putten et al. [215] used a comb to increase the surface roughness of the deposited layer and create the interlayer interlocking manually. Positive results were also determined in their case. Recently, Van Overmeir [218] equipped a comb/brush on the nozzle to automatically generate the interlayer interlocking. As recommended by the author, adding the comb/brush shape should be considered for the future nozzle design.

(2) Increasing the adhesion between layers

Applying a thin layer of cementitious ‘glue’ paste between two subsequent layers is also an effective way to improve the interlayer bond strength. This method is particularly suitable for material exhibiting high stiffness and weak intermixing after deposition. A twin-nozzle printhead that can fully employ this concept (one nozzle for general material layer and another for cementitious ‘glue’ paste) was proposed by Marchment et al. [216]. The authors also found that the high and sustained flowable OPC paste could significantly enhance the bond strength. This is attributed to the presence of a greater malleable surface area for creating an effective contact area achieved by the mixture with a higher flowability. A similar approach was applied by Ma et al. [219], whereas the ‘glue’ material in their case was a blend of OPC and high-belite CSA cement-based mortar. In their additive mortar, cellulose fiber was added as an internal curing agent, and fine limestone filler was used for adjusting the workability and hydration.

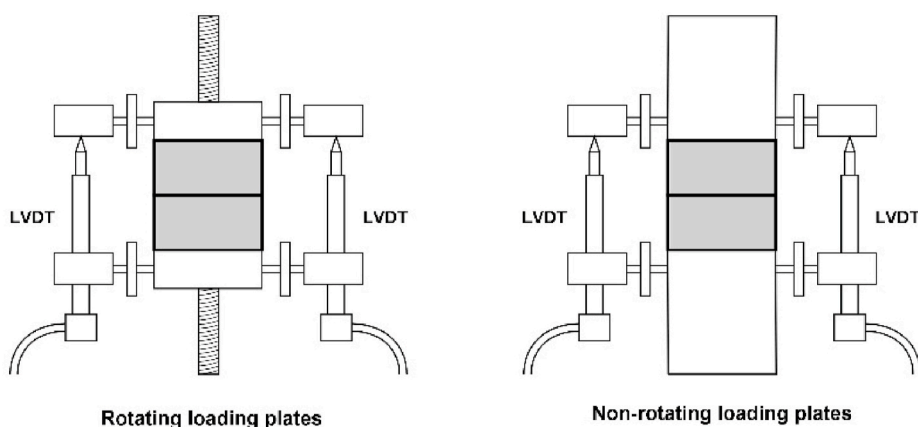


Fig. 15. Uniaxial tensile test setup with rotating loading plates (Left) and non-rotating loading plates (Right).

4.2.2. Characterization of void/unfilled area

During the 3DCP process, many voids may be entrapped between filaments. This phenomenon was observed by Le et al. [214] for the first time. They found that a void in the range of 0.2–4 mm diameter may be formed between four consecutive filaments by using a nozzle with a round opening. Buswell et al. [1] pointed out that the formation of the void depends mainly on the rheology of printable cementitious materials, predefined printing path, and the geometry of nozzle opening. Recently, the macropores/voids that appeared at the interface of two layers were highlighted by studies [26,44,56,101,207]. The presence of these voids seems to be the main reason resulting in the weak interlayer bond strength and anisotropy of printed cementitious materials, as mentioned in Section 4.2.1.1. Additionally, the entrapped air voids in the layer area induced by the pumping and extrusion process were also characterized by works [220,221]. The content, size, and distribution of these air voids can influence the mechanical performance and the durability of the printed cementitious materials, such as freeze-thaw and scaling [222]. Thus, it is essential to characterize the void system of 3D printed cementitious materials.

Generally, three main approaches have been used to investigate the voids/macropores structure of the printed sample.

First, the air voids at the interface of two subsequent layers can be directly observed under scanning electron microscope (SEM), according to Refs. [207,210]. This method is a qualitative way to characterize voids. To quantify the air-void content, SEM may not be an ideal tool due to its limited observation field.

Second, for mold-cast cementitious materials, the stereological examination of polished samples or thin sections using a flatbed scanner or optical microscope was employed to rapidly quantify air voids via approaches, including point-count and linear-traverse methods based on ASTM C457-98 [223] or NEN-EN 480-11 [224]. For exploring the impacts of pumping and extrusion processes on the air void structure of 3D printed mortar, Das et al. [221] prepared their samples and performed the image analysis in accordance with ASTM C457-98 [223]. However, in their case, the polished sections were sourced from the mold-cast cylindrical samples, and therefore, the interface properties cannot be studied. Chen et al. [220] extracted thin sections with relatively small sample fields (four layers, $35 \times 14.6 \text{ mm}^2$) from 3D printed samples (see Fig. 16). The air voids in both layer and interface regions were characterized in their study. The authors found that most of air voids (100–6000 μm) were recognized as irregular and elongated morphology induced by the extrusion and layer-wise 3DCP process. Due to the 2D effects, the characterization of air-void content, size, and shape using polished/thin sections (optical microscopy/image scanning) may be inadequate to reflect the 'real' air-void structure of printed cementitious materials.

Third, for assessing 3D heterogeneity of air void structure, X-ray computed tomography (CT) can be implemented. Using CT scanning and image analysis techniques for characterizing air void systems of mold-cast cementitious materials have been conducted by many earlier studies [225–229]. Recently, researchers [5,26,101,209,220,230] also employed these approaches to quantify the air void content of 3D printed cementitious materials for investigating the effects of different printing parameters or materials on inter-layer properties. In 3D configuration, an elongated morphology of the air void volume can be observed, as shown in Fig. 17. However, the accuracy of image analysis is primarily dependent on the resolution of acquired images. The maximum resolution of obtained grey-scale value images via CT scanning, which is limited by the sample dimension, may be lower than that of the polished/thin section for acquiring the same region of interest (ROI). Thus, in this context, the very small air voids that can be characterized by optical microscopy/image scanning may not be captured by using CT scanning. Besides, as CT scanning is not a method that can be found/used easily, the stereological examination is still the most generic way in the industry.

5. Summary and perspectives

Based on the information discussed in this study, the conclusions and perspectives could be made as follows.

(1) Printing strategy:

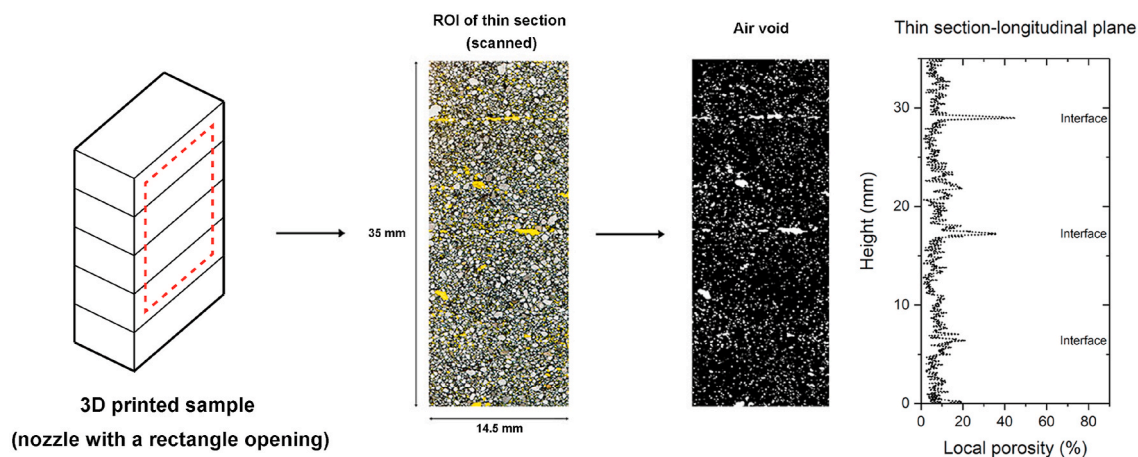


Fig. 16. Air void characterization by using optical image scanning (thin section) and image analysis, adapted from Ref. [220].

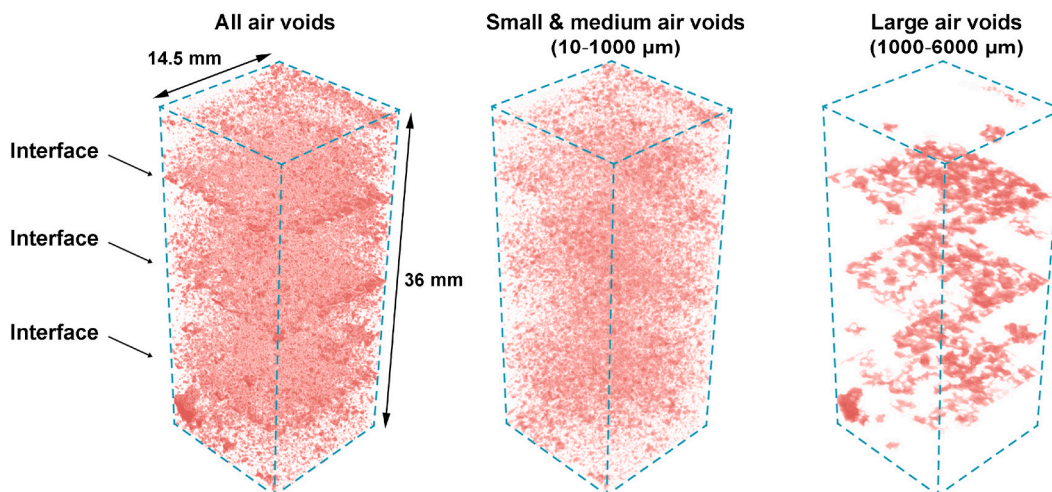


Fig. 17. 3D visualization of the air voids in the 3D printed sample obtained by using CT scanning, adapted from Ref. [220].

- Extrusion of very high/sufficiently stiff materials is still the most common printing strategy in the field of 3DCP. However, the pumping distance for extrusion of stiff materials is limited due to the high pumping pressure induced by the high yield stress and plastic viscosity.
 - Compared to the very high/sufficiently stiff material, the material for set-on-demand printing exhibits exceptionally high fluidity during mixing, pumping, and extrusion processes, which may be more suitable for large-scale construction projects. However, the study of set-on-demand printing is still limited and requires further investigations.
- (2) Sustainable cementitious materials:
- Physical and chemical characteristics of SCMs were generally believed as the main reason for influencing the rheology of fresh mixtures.
 - Compared with fly ash, slag, and silica fume, calcined clay and limestone appear to be suitable alternatives to common SCMs for developing sustainable cementitious materials in the longer term. Feasibility of using high volumes of limestone and calcined clay as cement substitutions in 3DCP needs further research. The variables of calcined clay, including the MK content, secondary phase, fineness, SSA, morphology, and the presence of uncalcined kaolinitic clay or swelling clays, could strongly influence the fresh and hardened properties of the blended cementitious materials.
- (3) Characterization methods
- For characterizing the fresh properties of printable cementitious materials during the pumping, and extrusion processes, offline methods, like flowability, ram extrusion, and rheometry (CSR/hysteresis loop) tests can be employed. The inline measurements, including pumpability, extrudability, and open time tests, are also necessary to be applied for validating the printability of developed mixtures.
 - After material deposition, the quantification of buildability and structural build-up becomes critical. Development of yield stress/stiffness with time can be quantitatively determined using the green strength test, penetration test, and rheometry (static yield stress measurement with time, SAOS, and LAOS tests). The inline buildability test incorporating experiment monitoring systems can be implemented to evaluate the developed mixtures directly.
 - Next to the effect of material compositions, printing parameters, i.e., time intervals, nozzle standoff distances, printing environmental conditions, and nozzle types, can also affect the interlayer bond strength of printed cementitious materials. Additionally, the current strategies for enhancing interlayer bonding can be summarized as increasing the contact area (for instance by interlocking), and the adhesion between layers.
 - Since standards, norms, and guidelines for 3D printable cementitious materials do currently not exist, standard tests specifically for quantifying the fresh properties and interlayer behaviors of such materials are desired.
 - The presence of air voids appears to be an important reason for weak interlayer bond strength and anisotropy of printed cementitious materials. The air voids in 3D printed samples can be quantitatively characterized using optical image scanning and X-ray computed tomography.

Author statement

Yu Chen: Formal analysis; Visualization; Writing - original draft; Writing - review & editing. Shan He: Writing - review & editing. Yidong Gan: Writing - review & editing. Oğuzhan Çopuroğlu: Supervision; Writing - review & editing. Fred Veer: Supervision; Writing - review & editing. Erik Schlangen: Supervision; Funding acquisition; Writing - review & editing.

Declaration of competing interest

The authors declare that they have no known competing financial interests or personal relationships that could have appeared to influence the work reported in this paper.

Acknowledgments

Yu Chen and Yidong Gan would like to acknowledge the funding supported by China Scholarship Council under grant No. 201807720005 and 201706130140.

References

- [1] R.A. Buswell, W.R. Leal de Silva, S.Z. Jones, J. Dirrenberger, 3D printing using concrete extrusion: a roadmap for research, *Cement Concr. Res.* 112 (2018) 37–49, <https://doi.org/10.1016/j.cemconres.2018.05.006>.
- [2] V. Mechtcherine, F.P. Bos, A. Perrot, W.R.L. da Silva, V.N. Nerella, S. Fataei, R.J.M. Wolfs, M. Sonebi, N. Roussel, Extrusion-based additive manufacturing with cement-based materials – production steps, processes, and their underlying physics: a review, *Cement Concr. Res.* 132 (2020) 106037, <https://doi.org/10.1016/j.cemconres.2020.106037>.
- [3] V. Mechtcherine, V.N. Nerella, F. Will, M. Näther, J. Otto, M. Krause, Large-scale digital concrete construction – CONPrint3D concept for on-site, monolithic 3D-printing, *Autom. ConStruct.* 107 (2019) 102933, <https://doi.org/10.1016/j.autcon.2019.102933>.
- [4] R.J.M. Wolfs, F.P. Bos, T.A.M. Salet, Hardened properties of 3D printed concrete: the influence of process parameters on interlayer adhesion, *Cement Concr. Res.* 119 (2019) 132–140, <https://doi.org/10.1016/j.cemconres.2019.02.017>.
- [5] Y. Chen, K. Jansen, H. Zhang, C. Romero Rodriguez, Y. Gan, O. Çopuroğlu, E. Schlangen, Effect of printing parameters on interlayer bond strength of 3D printed limestone-calcined clay-based cementitious materials: an experimental and numerical study, *Construct. Build. Mater.* 262 (2020), 120094, <https://doi.org/10.1016/j.conbuildmat.2020.120094>.
- [6] Y. Chen, F. Veer, O. Çopuroğlu, A critical review of 3D concrete printing as a low CO₂ concrete approach, *Heron* 62 (2017) 167–194.
- [7] B. Panda, S.C. Paul, L.J. Hui, Y.W.D. Tay, M.J. Tan, Additive manufacturing of geopolymer for sustainable built environment, *J. Clean. Prod.* 167 (2017) 281–288, <https://doi.org/10.1016/j.jclepro.2017.08.165>.
- [8] Y. Chen, F. Veer, O. Copuroglu, E. Schlangen, Feasibility of using low CO₂ concrete alternatives in extrusion-based 3D concrete printing, in: R. Flatt, T. Wangler (Eds.), *RILEM Int. Conf. Concr. Digit. Fabr.*, 2018, pp. 269–276, Zurich.
- [9] J.J. Biernacki, J.W. Bullard, G. Sant, K. Brown, F.P. Glasser, S. Jones, T. Ley, R. Livingston, L. Nicoleau, J. Olek, F. Sanchez, R. Shahsavari, P.E. Stutzman, K. Sobolev, T. Prater, Cements in the 21st century: challenges, perspectives, and opportunities, *J. Am. Ceram. Soc.* 100 (2017) 2746–2773, <https://doi.org/10.1111/jace.14948>.
- [10] A.R. Arunothayan, B. Nematollahi, R. Ranade, S.H. Bong, J.G. Sanjayan, K.H. Khayat, Fiber orientation effects on ultra-high performance concrete formed by 3D printing, *Cement Concr. Res.* 143 (2021) 106384, <https://doi.org/10.1016/j.cemconres.2021.106384>.
- [11] G. Vantghem, W. De Corte, E. Shakour, O. Amir, 3D printing of a post-tensioned concrete girder designed by topology optimization, *Autom. ConStruct.* 112 (2020) 103084, <https://doi.org/10.1016/j.autcon.2020.103084>.
- [12] I. Agusti-Juan, G. Habert, Environmental design guidelines for digital fabrication, *J. Clean. Prod.* 142 (2017) 2780–2791, <https://doi.org/10.1016/j.jclepro.2016.10.190>.
- [13] G. De Schutter, K. Lesage, V. Mechtcherine, V.N. Nerella, G. Habert, I. Agusti-Juan, Vision of 3D printing with concrete — technical, economic and environmental potentials, *Cement Concr. Res.* 112 (2018) 25–36, <https://doi.org/10.1016/j.cemconres.2018.06.001>.
- [14] A.M. Rashad, An overview on rheology, mechanical properties and durability of high-volume slag used as a cement replacement in paste, mortar and concrete, *Construct. Build. Mater.* 187 (2018) 89–117, <https://doi.org/10.1016/j.conbuildmat.2018.07.150>.
- [15] A.M. Rashad, A brief on high-volume Class F fly ash as cement replacement – a guide for Civil Engineer, *Int. J. Sustain. Built Environ.* 4 (2015) 278–306, <https://doi.org/10.1016/J.IJSBE.2015.10.002>.
- [16] A.M. Rashad, Metakaolin as cementitious material: history, scours, production and composition – a comprehensive overview, *Construct. Build. Mater.* 41 (2013) 303–318, <https://doi.org/10.1016/j.conbuildmat.2012.12.001>.
- [17] A.M. Rashad, An overview of pumice stone as a cementitious material – the best manual for civil engineer, *Silicon* 2020 132 13 (2020) 551–572, <https://doi.org/10.1007/S12633-020-00469-3>.
- [18] A.M. Rashad, A brief review on blast-furnace slag and copper slag as fine aggregate in mortar and concrete based on portland cement, *Rev. Adv. Mater. Sci.* 44 (2016), 221–127.
- [19] T. Ding, J. Xiao, S. Zou, Y. Wang, Hardened properties of layered 3D printed concrete with recycled sand, *Cement Concr. Compos.* 113 (2020) 103724, <https://doi.org/10.1016/j.cemconcomp.2020.103724>.
- [20] T. Ding, J. Xiao, F. Qin, Z. Duan, Mechanical behavior of 3D printed mortar with recycled sand at early ages, *Construct. Build. Mater.* 248 (2020) 118654, <https://doi.org/10.1016/j.conbuildmat.2020.118654>.
- [21] J. Xiao, S. Zou, Y. Yu, Y. Wang, T. Ding, Y. Zhu, J. Yu, S. Li, Z. Duan, Y. Wu, L. Li, 3D recycled mortar printing: system development, process design, material properties and on-site printing, *J. Build. Eng.* 32 (2020) 101779, <https://doi.org/10.1016/j.jobee.2020.101779>.
- [22] X. Li, N. Zhang, J. Yuan, X. Wang, Y. Zhang, F. Chen, Y. Zhang, Preparation and microstructural characterization of a novel 3D printable building material composed of copper tailings and iron tailings, *Construct. Build. Mater.* 249 (2020) 118779, <https://doi.org/10.1016/j.conbuildmat.2020.118779>.
- [23] G. Ma, Z. Li, L. Wang, Printable properties of cementitious material containing copper tailings for extrusion based 3D printing, *Construct. Build. Mater.* 162 (2018) 613–627, <https://doi.org/10.1016/j.conbuildmat.2017.12.051>.
- [24] S. Lim, R.A. Buswell, T.T. Le, S.A. Austin, A.G.F. Gibb, T. Thorpe, Developments in construction-scale additive manufacturing processes, *Autom. ConStruct.* (2012), <https://doi.org/10.1016/j.autcon.2011.06.010>.
- [25] T.T. Le, S.A. Austin, S. Lim, R.A. Buswell, A.G.F. Gibb, T. Thorpe, Mix design and fresh properties for high-performance printing concrete, *Mater. Struct. Constr.* 45 (2012) 1221–1232, <https://doi.org/10.1617/s11527-012-9828-z>.
- [26] Y. Chen, S. Chaves Figueiredo, Z. Li, Z. Chang, K. Jansen, O. Çopuroğlu, E. Schlangen, Improving printability of limestone-calcined clay-based cementitious materials by using viscosity-modifying admixture, *Cement Concr. Res.* 132 (2020) 106040, <https://doi.org/10.1016/j.cemconres.2020.106040>.
- [27] R. Wolfs, Experimental Characterization and Numerical Modelling of 3D Printed Concrete, Eindhoven University of Technology, 2019.
- [28] N. Roussel, Rheological requirements for printable concretes, *Cement Concr. Res.* 112 (2018) 76–85, <https://doi.org/10.1016/j.cemconres.2018.04.005>.
- [29] F. Bos, R. Wolfs, Z. Ahmed, T. Salet, Additive manufacturing of concrete in construction: potentials and challenges of 3D concrete printing, *Virtual Phys. Prototyp.* 11 (2016) 209–225, <https://doi.org/10.1080/17452759.2016.1209867>.
- [30] C. Gosselin, R. Duballet, P. Roux, N. Gaudillière, J. Dirrenberger, P. Morel, Large-scale 3D printing of ultra-high performance concrete - a new processing route for architects and builders, *Mater. Des.* 100 (2016) 102–109, <https://doi.org/10.1016/j.matdes.2016.03.097>.
- [31] L. Reiter, T. Wangler, N. Roussel, R.J. Flatt, The role of early age structural build-up in digital fabrication with concrete, *Cement Concr. Res.* 112 (2018) 86–95, <https://doi.org/10.1016/j.cemconres.2018.05.011>.
- [32] L. Reiter, T. Wangler, A. Anton, R.J. Flatt, Setting on demand for digital concrete – principles, measurements, chemistry, validation, *Cement Concr. Res.* 132 (2020) 106047, <https://doi.org/10.1016/j.cemconres.2020.106047>.
- [33] D. Marchon, S. Kawashima, H. Bessaies-Bey, S. Mantellato, S. Ng, Hydration and rheology control of concrete for digital fabrication: potential admixtures and cement chemistry, *Cement Concr. Res.* 112 (2018) 96–110, <https://doi.org/10.1016/j.cemconres.2018.05.014>.

- [34] W.R. Leal da Silva, H. Fryda, J.-N. Bousseau, P.-A. Andreani, T.J. Andersen, Evaluation of early-age concrete structural build-up for 3D concrete printing by oscillatory rheometry, in: *Adv. Intell. Syst. Comput.*, 2020, pp. 35–47, https://doi.org/10.1007/978-3-030-20216-3_4.
- [35] V. Esmault, A. Labyad, M. Chantini, F. Toussaint, Experience in online modification of rheology and strength acquisition of 3D printable mortars, in: T. Wangler, R. Flatt (Eds.), *First RILEM Int. Conf. Concr. Digit. Fabr. – Digit. Concr.*, Springer International Publishing, 2019, pp. 24–38, https://doi.org/10.1007/978-3-319-99519-9_3.
- [36] T. Wangler, *Digital concrete: research and applications*, *Proc. 10th Int. Concr. Congr.* (2019) 2–12.
- [37] C. Meyer, The greening of the concrete industry, *Cement Concr. Compos.* 31 (2009) 601–605, <https://doi.org/10.1016/j.cemconcomp.2008.12.010>.
- [38] V. Malhotra, Role of supplementary cementing materials in reducing greenhouse gas emissions, in: *Concr. Technol. A Sustain. Dev. 21st Century*, E&FN Spon, London, 1999, pp. 226–235.
- [39] P. Van Den Heede, N. De Belie, Environmental impact and life cycle assessment (LCA) of traditional and ‘green’ concretes: literature review and theoretical calculations, *Cement Concr. Compos.* 34 (2012) 431–442, <https://doi.org/10.1016/J.CEMCONCOMP.2012.01.004>.
- [40] K. Mehta, P.J.M. Monteiro, *Concrete: Microstructure, Properties, and Materials*, third ed., McGraw-Hill, New York, 2006, <https://doi.org/10.1036/0071462899>.
- [41] M.K. Mohan, A.V. Rahul, K. Van Tittelboom, G. De Schutter, Rheological and pumping behaviour of 3D printable cementitious materials with varying aggregate content, *Cement Concr. Res.* 139 (2021) 106258, <https://doi.org/10.1016/j.cemconres.2020.106258>.
- [42] C. Zhang, Z. Hou, C. Chen, Y. Zhang, V. Mechtcherine, Z. Sun, Design of 3D printable concrete based on the relationship between flowability of cement paste and optimum aggregate content, *Cement Concr. Compos.* 104 (2019) 103406, <https://doi.org/10.1016/j.cemconcomp.2019.103406>.
- [43] B. Panda, S. Ruan, C. Unluer, M.J. Tan, Improving the 3D printability of high volume fly ash mixtures via the use of nano attapulgite clay, *Compos. B Eng.* 165 (2019) 75–83, <https://doi.org/10.1016/j.compositesb.2018.11.109>.
- [44] Y.W.D. Tay, G.H.A. Ting, Y. Qian, B. Panda, L. He, M.J. Tan, Time gap effect on bond strength of 3D-printed concrete, *Virtual Phys. Prototyp.* 14 (2019) 104–113, <https://doi.org/10.1080/17452759.2018.1500420>.
- [45] Y.W.D. Tay, M.Y. Li, M.J. Tan, Effect of printing parameters in 3D concrete printing: printing region and support structures, *J. Mater. Process. Technol.* 271 (2019) 261–270, <https://doi.org/10.1016/j.jmatprotec.2019.04.007>.
- [46] A.V. Rahul, A. Sharma, M. Santhanam, A desorptivity-based approach for the assessment of phase separation during extrusion of cementitious materials, *Cement Concr. Compos.* 108 (2020) 103546, <https://doi.org/10.1016/j.cemconcomp.2020.103546>.
- [47] S.C. Paul, Y.W.D. Tay, B. Panda, M.J. Tan, Fresh and hardened properties of 3D printable cementitious materials for building and construction, *Arch. Civ. Mech. Eng.* 18 (2018) 311–319, <https://doi.org/10.1016/j.acme.2017.02.008>.
- [48] B. Panda, M.J. Tan, Rheological behavior of high volume fly ash mixtures containing micro silica for digital construction application, *Mater. Lett.* 237 (2019) 348–351, <https://doi.org/10.1016/j.matlet.2018.11.131>.
- [49] B. Panda, M.J. Tan, Material properties of 3D printable high-volume slag cement, in: *First Int. Conf. 3D Constr. Print. Conjunction with 6th Int. Conf. Innov. Prod. Constr (IPC 2018)*, 2018.
- [50] V.N. Nerella, M. Näther, A. Iqbal, M. Butler, V. Mechtcherine, Inline quantification of extrudability of cementitious materials for digital construction, *Cement Concr. Compos.* 95 (2019) 260–270, <https://doi.org/10.1016/j.cemconcomp.2018.09.015>.
- [51] A. Kazemian, X. Yuan, E. Cochran, B. Khoshnevis, Cementitious materials for construction-scale 3D printing: laboratory testing of fresh printing mixture, *Construct. Build. Mater.* 145 (2017) 639–647, <https://doi.org/10.1016/j.conbuildmat.2017.04.015>.
- [52] A.V. Rahul, M. Santhanam, H. Meena, Z. Ghani, 3D printable concrete: mixture design and test methods, *Cement Concr. Compos.* 97 (2019) 13–23, <https://doi.org/10.1016/j.cemconcomp.2018.12.014>.
- [53] Y. Weng, M. Li, M.J. Tan, S. Qian, Design 3D printing cementitious materials via Fuller Thompson theory and Marson-Percy model, *Construct. Build. Mater.* 163 (2018) 600–610, <https://doi.org/10.1016/j.conbuildmat.2017.12.112>.
- [54] Y. Zhang, Y. Zhang, G. Liu, Y. Yang, M. Wu, B. Pang, Fresh properties of a novel 3D printing concrete ink, *Construct. Build. Mater.* 174 (2018) 263–271, <https://doi.org/10.1016/j.conbuildmat.2018.04.115>.
- [55] B. Panda, J.H. Lim, M.J. Tan, Mechanical properties and deformation behaviour of early age concrete in the context of digital construction, *Compos. B Eng.* 165 (2019) 563–571, <https://doi.org/10.1016/j.compositesb.2019.02.040>.
- [56] B. Panda, N.A.N. Mohamed, S.C. Paul, G.V.P.B. Singh, M.J. Tan, B. Šavija, The effect of material fresh properties and process parameters on buildability and interlayer adhesion of 3D printed concrete, *Materials* 12 (2019) 2149, <https://doi.org/10.3390/ma12132149>.
- [57] Y. Chen, Z. Li, S. Chaves Figueiredo, O. Çopuroğlu, F. Veer, E. Schlangen, Limestone and calcined clay-based sustainable cementitious materials for 3D concrete printing: a fundamental study of extrudability and early-age strength development, *Appl. Sci.* 9 (2019) 1809, <https://doi.org/10.3390/app9091809>.
- [58] Z. Giergiczny, Fly ash and slag, *Cement Concr. Res.* 124 (2019), <https://doi.org/10.1016/j.cemconres.2019.105826>.
- [59] K. Sideris, H. Justnes, M. Soutsos, T. Sui, Fly ash, in: N. De Belie, M. Soutsos, E. Gruyaert (Eds.), *Prop. Fresh Hardened Concr. Contain. Suppl. Cem. Mater.*, Springer, Cham, 2018, pp. 55–98, https://doi.org/10.1007/978-3-319-70606-1_2.
- [60] I. Domanskaya, V. Oleinik, Peculiarities of formation of phase structure and the hydraulic activity of high-calcium fly ash, in: C. Brebbia, J. Connor (Eds.), *Prog. Mater. Sci. Eng. Innov. Discov. Russ. Sci. Eng.*, Springer, Cham, 2018, pp. 149–154, https://doi.org/10.1007/978-3-319-75340-9_19.
- [61] D. Jiao, C. Shi, Q. Yuan, X. An, Y. Liu, H. Li, Effect of constituents on rheological properties of fresh concrete-A review, *Cement Concr. Compos.* 83 (2017) 146–159, <https://doi.org/10.1016/j.cemconcomp.2017.07.016>.
- [62] A. Beycioğlu, H. Yılmaz Aruntaş, Workability and mechanical properties of self-compacting concretes containing LLFA, GBFS and MC, *Construct. Build. Mater.* 73 (2014) 626–635, <https://doi.org/10.1016/j.conbuildmat.2014.09.071>.
- [63] M. Jalal, M. Fathi, M. Farzad, Effects of fly ash and TiO₂ nanoparticles on rheological, mechanical, microstructural and thermal properties of high strength self compacting concrete, *Mech. Mater.* 61 (2013) 11–27, <https://doi.org/10.1016/j.mechmat.2013.01.010>.
- [64] S.C. Paul, Y.W.D. Tay, B. Panda, M.J. Tan, Fresh and hardened properties of 3D printable cementitious materials for building and construction, *Arch. Civ. Mech. Eng.* 18 (2018) 311–319, <https://doi.org/10.1016/j.acme.2017.02.008>.
- [65] S. Chaves Figueiredo, C. Romero Rodríguez, Z.Y. Ahmed, D.H. Bos, Y. Xu, T.M. Salet, O. Çopuroğlu, E. Schlangen, F.P. Bos, An approach to develop printable strain hardening cementitious composites, *Mater. Des.* 169 (2019), <https://doi.org/10.1016/j.matdes.2019.107651>.
- [66] M.C.G. Juenger, R. Snellings, S.A. Bernal, Supplementary cementitious materials: new sources, characterization, and performance insights, *Cement Concr. Res.* 122 (2019) 257–273, <https://doi.org/10.1016/j.cemconres.2019.05.008>.
- [67] I. Yuksel, Blast-furnace slag, in: *Waste Suppl. Cem. Mater. Concr. Characterisation*, Prop. Appl., Elsevier Ltd, 2018, pp. 361–415, <https://doi.org/10.1016/B978-0-08-102156-9.00012-2>.
- [68] EN 197-1, *Cement - Part 1: Composition, Specifications and Conformity Criteria for Common Cements*, NEN, 2000, pp. 178–184, [https://doi.org/10.1016/0005-2736\(80\)90400-9](https://doi.org/10.1016/0005-2736(80)90400-9).
- [69] C.K. Park, M.H. Noh, T.H. Park, Rheological properties of cementitious materials containing mineral admixtures, *Cement Concr. Res.* 35 (2005) 842–849, <https://doi.org/10.1016/j.cemconres.2004.11.002>.
- [70] R.S. Ahari, T.K. Erdem, K. Ramyar, Thixotropy and structural breakdown properties of self consolidating concrete containing various supplementary cementitious materials, *Cement Concr. Compos.* 59 (2015) 26–37, <https://doi.org/10.1016/j.cemconcomp.2015.03.009>.
- [71] B. Panda, S. Ruan, C. Unluer, M.J. Tan, Investigation of the properties of alkali-activated slag mixes involving the use of nanoclay and nucleation seeds for 3D printing, *Compos. B Eng.* 186 (2020) 107826, <https://doi.org/10.1016/j.compositesb.2020.107826>.
- [72] H. Alghamdi, S.A.O. Nair, N. Neithalath, Insights into material design, extrusion rheology, and properties of 3D-printable alkali-activated fly ash-based binders, *Mater. Des.* 167 (2019) 107634, <https://doi.org/10.1016/j.matdes.2019.107634>.
- [73] B. Panda, C. Unluer, M.J. Tan, Investigation of the rheology and strength of geopolymer mixtures for extrusion-based 3D printing, *Cement Concr. Compos.* 94 (2018) 307–314, <https://doi.org/10.1016/j.cemconcomp.2018.10.002>.
- [74] Z. Li, L. Wang, G. Ma, Mechanical improvement of continuous steel microcable reinforced geopolymer composites for 3D printing subjected to different loading conditions, *Compos. B Eng.* 187 (2020) 107796, <https://doi.org/10.1016/j.compositesb.2020.107796>.

- [75] S. Bong, B. Nematollahi, A. Nazari, M. Xia, J. Sanjayan, Method of optimisation for ambient temperature cured sustainable geopolymers for 3D printing construction applications, *Materials* 12 (2019) 902, <https://doi.org/10.3390/ma12060902>.
- [76] C. Sun, J. Xiang, M. Xu, Y. He, Z. Tong, X. Cui, 3D extrusion free forming of geopolymer composites: materials modification and processing optimization, *J. Clean. Prod.* 258 (2020), 120986, <https://doi.org/10.1016/j.jclepro.2020.120986>.
- [77] P. Nanthagopalan, M. Haist, M. Santhanam, H.S. Müller, Investigation on the influence of granular packing on the flow properties of cementitious suspensions, *Cement Concr. Compos.* 30 (2008) 763–768, <https://doi.org/10.1016/j.cemconcomp.2008.06.005>.
- [78] M. Benaicha, X. Roguiez, O. Jalbaud, Y. Burtshell, A.H. Alaoui, Influence of silica fume and viscosity modifying agent on the mechanical and rheological behavior of self compacting concrete, *Construct. Build. Mater.* 84 (2015) 103–110, <https://doi.org/10.1016/j.conbuildmat.2015.03.061>.
- [79] M. Nehdi, S. Mindess, P.C. Aitcin, Rheology of high-performance concrete: effect of ultrafine particles, *Cement Concr. Res.* 28 (1998) 687–697, [https://doi.org/10.1016/S0008-8846\(98\)00022-2](https://doi.org/10.1016/S0008-8846(98)00022-2).
- [80] A.I. Laskar, S. Talukdar, Rheological behavior of high performance concrete with mineral admixtures and their blending, *Construct. Build. Mater.* 22 (2008) 2345–2354, <https://doi.org/10.1016/j.conbuildmat.2007.10.004>.
- [81] N. Roussel, Rheology of fresh concrete: from measurements to predictions of casting processes, *Mater. Struct. Constr.* 40 (2007) 1001–1012, <https://doi.org/10.1617/s11527-007-9313-2>.
- [82] N. Roussel, A thixotropy model for fresh fluid concretes: theory, validation and applications, *Cement Concr. Res.* (2006), <https://doi.org/10.1016/j.cemconres.2006.05.025>.
- [83] M.K. Rahman, M.H. Baluch, M.A. Malik, Thixotropic behavior of self compacting concrete with different mineral admixtures, *Construct. Build. Mater.* 50 (2014) 710–717, <https://doi.org/10.1016/j.conbuildmat.2013.10.025>.
- [84] Z. Liu, M. Li, Y. Weng, T.N. Wong, M.J. Tan, Mixture Design Approach to optimize the rheological properties of the material used in 3D cementitious material printing, *Construct. Build. Mater.* 198 (2019) 245–255, <https://doi.org/10.1016/j.conbuildmat.2018.11.252>.
- [85] X. Zhang, J. Han, The effect of ultra-fine admixture on the rheological property of cement paste, *Cement Concr. Res.* 30 (2000) 827–830, [https://doi.org/10.1016/S0008-8846\(00\)00236-2](https://doi.org/10.1016/S0008-8846(00)00236-2).
- [86] R. Saleh Ahari, T. Kemal Erdem, K. Ramyar, Effect of various supplementary cementitious materials on rheological properties of self-consolidating concrete, *Construct. Build. Mater.* 75 (2015) 89–98, <https://doi.org/10.1016/j.conbuildmat.2014.11.014>.
- [87] B. Lu, Y. Weng, M. Li, Y. Qian, K.F. Leong, M.J. Tan, S. Qian, A systematical review of 3D printable cementitious materials, *Construct. Build. Mater.* 207 (2019) 477–490, <https://doi.org/10.1016/j.conbuildmat.2019.02.144>.
- [88] Z. Li, L. Wang, G. Ma, Method for the enhancement of buildability and bending resistance of 3D printable tailing mortar, *Int. J. Concr. Struct. Mater.* (2018), <https://doi.org/10.1186/s40069-018-0269-0>.
- [89] B. Lothenbach, K. Scrivener, R.D. Hooton, Supplementary cementitious materials, *Cement Concr. Res.* (2011), <https://doi.org/10.1016/j.cemconres.2010.12.001>.
- [90] K. Scrivener, F. Martirena, S. Bishnoi, S. Maity, Calcined clay limestone cements (LC3), *Cement Concr. Res.* 114 (2018) 49–56, <https://doi.org/10.1016/j.cemconres.2017.08.017>.
- [91] R. Snellings, Assessing, understanding and unlocking supplementary cementitious materials, *RILEM Tech. Lett.* 1 (2016) 50, <https://doi.org/10.21809/rilemtechlett.2016.12>.
- [92] D.P. Bentz, S.Z. Jones, I.R. Bentz, M.A. Peltz, Towards the formulation of robust and sustainable cementitious binders for 3-D additive construction by extrusion, *Construct. Build. Mater.* 175 (2018) 215–224, <https://doi.org/10.1016/j.conbuildmat.2018.04.167>.
- [93] K. Vance, A. Kumar, G. Sant, N. Neithalath, The rheological properties of ternary binders containing Portland cement, limestone, and metakaolin or fly ash, *Cement Concr. Res.* 52 (2013) 196–207, <https://doi.org/10.1016/j.cemconres.2013.07.007>.
- [94] K. Ma, G. Long, Y. Xie, R. Zhu, Rheological properties of compound pastes with cement-fly ash-limestone powder, *J. Chin. Ceram. Soc.* 41 (2013) 582–587, <https://doi.org/10.7521/j.issn.0454-5648.2013.05.02>.
- [95] D.P. Bentz, T. Sato, I. De La Varga, W.J. Weiss, Fine limestone additions to regulate setting in high volume fly ash mixtures, *Cement Concr. Compos.* 34 (2012) 11–17, <https://doi.org/10.1016/j.cemconcomp.2011.09.004>.
- [96] E. Berodier, K. Scrivener, Understanding the filler effect on the nucleation and growth of C-S-H, *J. Am. Ceram. Soc.* 97 (2014) 3764–3773, <https://doi.org/10.1111/jace.13177>.
- [97] T. Matschei, B. Lothenbach, F.P. Glasser, The role of calcium carbonate in cement hydration, *Cement Concr. Res.* 37 (2007) 551–558, <https://doi.org/10.1016/j.cemconres.2006.10.013>.
- [98] Y. Tao, K. Lesage, K. Van Tittelboom, Y. Yuan, G. De Schutter, Effect of limestone powder substitution on fresh and hardened properties of 3D printable mortar, in: F. Bos, S. Lucas, R. Wolfs, T. Salet (Eds.), *Second RILEM Int. Conf. Concr. Digit. Fabr. – Digit. Concr.* 2020, Springer, Cham, 2020, pp. 135–143, https://doi.org/10.1007/978-3-030-49916-7_14.
- [99] S. Chaves Figueiredo, C. Romero Rodríguez, Z.Y. Ahmed, D.H. Bos, Y. Xu, T.M. Salet, O. Çopuroğlu, E. Schlangen, F.P. Bos, Mechanical behavior of printed strain hardening cementitious composites, *Materials* 13 (2020) 2253, <https://doi.org/10.3390/ma13102253>.
- [100] S.A.O. Nair, H. Alghamdi, A. Arora, I. Mehdipour, G. Sant, N. Neithalath, Linking fresh paste microstructure, rheology and extrusion characteristics of cementitious binders for 3D printing, *J. Am. Ceram. Soc.* 102 (2019) 3951–3964, <https://doi.org/10.1111/jace.16305>.
- [101] Y. Chen, C.R. Rodríguez, Z. Li, B. Chen, O. Çopuroğlu, E. Schlangen, Effect of different grade levels of calcined clays on fresh and hardened properties of ternary-blended cementitious materials for 3D printing, *Cement Concr. Compos.* 114 (2020) 103708, <https://doi.org/10.1016/j.cemconcomp.2020.103708>.
- [102] K.L. Scrivener, Options for the future of cement, *Indian Concr. J.* 88 (2014) 11–21.
- [103] M. Antoni, J. Rossen, F. Martirena, K. Scrivener, Cement substitution by a combination of metakaolin and limestone, *Cement Concr. Res.* 42 (2012) 1579–1589, <https://doi.org/10.1016/j.cemconres.2012.09.006>.
- [104] R. San Nicolas, M. Cyr, G. Escadeillas, Characteristics and applications of flash metakaolins, *Appl. Clay Sci.* 83–84 (2013) 253–262, <https://doi.org/10.1016/j.clay.2013.08.036>.
- [105] W. Huang, H. Kazemi-Kamyab, W. Sun, K. Scrivener, Effect of replacement of silica fume with calcined clay on the hydration and microstructural development of eco-UHPC, *Mater. Des.* 121 (2017) 36–46, <https://doi.org/10.1016/j.matdes.2017.02.052>.
- [106] F. Avet, K. Scrivener, Investigation of the calcined kaolinite content on the hydration of limestone calcined clay cement (LC3), *Cement Concr. Res.* 107 (2018) 124–135, <https://doi.org/10.1016/j.cemconres.2018.02.016>.
- [107] F. Zunino, K. Scrivener, The reaction between metakaolin and limestone and its effect in porosity refinement and mechanical properties, *Cement Concr. Res.* 140 (2021) 106307, <https://doi.org/10.1016/j.cemconres.2020.106307>.
- [108] Y. Dhandapani, T. Sakthivel, M. Santhanam, R. Gettu, R.G. Pillai, Mechanical properties and durability performance of concretes with limestone calcined clay cement (LC 3), *Cement Concr. Res.* 107 (2018) 136–151, <https://doi.org/10.1016/j.cemconres.2018.02.005>.
- [109] F. Avet, R. Snellings, A. Alujas Diaz, M. Ben Haha, K. Scrivener, Development of a new rapid, relevant and reliable (R3) test method to evaluate the pozzolanic reactivity of calcined kaolinitic clays, *Cement Concr. Res.* 85 (2016) 1–11, <https://doi.org/10.1016/j.cemconres.2016.02.015>.
- [110] A. Alujas, R. Fernández, R. Quintana, K.L. Scrivener, F. Martirena, Pozzolanic reactivity of low grade kaolinitic clays: influence of calcination temperature and impact of calcination products on OPC hydration, *Appl. Clay Sci.* 108 (2015) 94–101, <https://doi.org/10.1016/j.clay.2015.01.028>.
- [111] J. Skibsted, R. Snellings, Reactivity of supplementary cementitious materials (SCMs) in cement blends, *Cement Concr. Res.* 124 (2019), <https://doi.org/10.1016/j.cemconres.2019.105799>.
- [112] M. Antoni, Investigation of cement substitution by blends of calcined clays and limestone, *Fac. Sci. Tech. L'Ingenieur. PhD* (2013) 254, <https://doi.org/10.5075/epfl-thesis-6001>.
- [113] H. Maraghechi, F. Avet, H. Wong, H. Kamyab, K. Scrivener, Performance of Limestone Calcined Clay Cement (LC3) with various kaolinite contents with respect to chloride transport, *Mater. Struct. Constr.* 51 (2018) 1–17, <https://doi.org/10.1617/s11527-018-1255-3>.
- [114] Z. Shi, M.R. Geiker, K. De Weerd, T.A. Østnor, B. Lothenbach, F. Winnefeld, J. Skibsted, Role of calcium on chloride binding in hydrated Portland cement–metakaolin–limestone blends, *Cement Concr. Res.* 95 (2017) 205–216, <https://doi.org/10.1016/j.cemconres.2017.02.003>.

- [115] Y. Dhandapani, M. Santhanam, Investigation on the microstructure-related characteristics to elucidate performance of composite cement with limestone-calcined clay combination, *Cement Concr. Res.* 129 (2020) 105959, <https://doi.org/10.1016/j.cemconres.2019.105959>.
- [116] F. Avet, *Investigation of the grade of calcined clays used as clinker substitute in Limestone Calcined Clay Cement (LC3)*, 8143, 2017, p. 169, Ph.D Thesis.
- [117] R. Siddique, J. Klaus, Influence of metakaolin on the properties of mortar and concrete: a review, *Appl. Clay Sci.* 43 (2009) 392–400, <https://doi.org/10.1016/j.clay.2008.11.007>.
- [118] Z. Shi, S. Ferreiro, B. Lothenbach, M.R. Geiker, W. Kunther, J. Kaufmann, D. Herfort, J. Skibsted, Sulfate resistance of calcined clay – limestone – Portland cements, *Cement Concr. Res.* 116 (2019) 238–251, <https://doi.org/10.1016/j.cemconres.2018.11.003>.
- [119] Q.D. Nguyen, T. Kim, A. Castel, Mitigation of alkali-silica reaction by limestone calcined clay cement (LC3), *Cement Concr. Res.* 137 (2020) 106176, <https://doi.org/10.1016/j.cemconres.2020.106176>.
- [120] M.F. Brigatti, E. Galán, B.K.G. Theng, *Structure and Mineralogy of Clay Minerals*, 2013, <https://doi.org/10.1016/B978-0-08-098258-8.00002-X>.
- [121] L. Lei, J. Plank, A study on the impact of different clay minerals on the dispersing force of conventional and modified vinyl ether based polycarboxylate superplasticizers, *Cement Concr. Res.* (2014), <https://doi.org/10.1016/j.cemconres.2014.02.009>.
- [122] D. Marchon, S. Mantellato, A.B. Eberhardt, R.J. Flatt, *Adsorption of Chemical Admixtures*, Elsevier Ltd, 2015, <https://doi.org/10.1016/B978-0-08-100693-1.00010-2>.
- [123] R. Sposito, N. Beuntner, K.-C. Thienel, Characteristics of calcined clay particles and their influence on the efficiency of superplasticizers, *Cement Concr. Compos.* 110 (2020) 103594, <https://doi.org/10.1016/j.cemconcomp.2020.103594>.
- [124] H. Paiva, A. Velosa, P. Cachim, V.M. Ferreira, Effect of metakaolin dispersion on the fresh and hardened state properties of concrete, *Cement Concr. Res.* 42 (2012) 607–612, <https://doi.org/10.1016/j.cemconres.2012.01.005>.
- [125] C. Perlot, P. Rougeau, S. Dehault, Slurry of metakaolin combined with limestone addition for self-compacted concrete. Application for precast industry, *Cement Concr. Compos.* 44 (2013) 50–57, <https://doi.org/10.1016/j.cemconcomp.2013.07.003>.
- [126] N. Nair, K. Mohammed Haneefa, M. Santhanam, R. Gettu, A study on fresh properties of limestone calcined clay blended cementitious systems, *Construct. Build. Mater.* 254 (2020) 119326, <https://doi.org/10.1016/j.conbuildmat.2020.119326>.
- [127] S. Ferreiro, D. Herfort, J.S. Damtoft, Effect of raw clay type, fineness, water-to-cement ratio and fly ash addition on workability and strength performance of calcined clay – limestone Portland cements, *Cement Concr. Res.* 101 (2017) 1–12, <https://doi.org/10.1016/j.cemconres.2017.08.003>.
- [128] F. Cassagnabère, P. Diederich, M. Mouret, G. Escadeillas, M. Lachemi, Impact of metakaolin characteristics on the rheological properties of mortar in the fresh state, *Cement Concr. Compos.* (2013), <https://doi.org/10.1016/j.cemconcomp.2012.12.001>.
- [129] M. Claverie, F. Martin, J.P. Tardy, M. Cyr, P. De Parseval, O. Grauby, C. Le Roux, Structural and chemical changes in kaolinite caused by flash calcination: formation of spherical particles, *Appl. Clay Sci.* 114 (2015) 247–255, <https://doi.org/10.1016/j.clay.2015.05.031>.
- [130] O. Akhlaghi, T. Aytas, B. Tatli, D. Sezer, A. Hodaie, A. Favier, K. Scrivener, Y.Z. Mencelolu, O. Akbulut, Modified poly(carboxylate ether)-based superplasticizer for enhanced flowability of calcined clay-limestone-gypsum blended Portland cement, *Cement Concr. Res.* 101 (2017) 114–122, <https://doi.org/10.1016/j.cemconres.2017.08.028>.
- [131] T.R. Muzenda, P. Hou, S. Kawashima, T. Sui, X. Cheng, The role of limestone and calcined clay on the rheological properties of LC3, *Cement Concr. Compos.* 107 (2020) 103516, <https://doi.org/10.1016/j.cemconcomp.2020.103516>.
- [132] M.A.B. Beigh, V.N. Nerella, E. Secrieru, V. Mechtcherine, Structural build-up behavior of limestone calcined clay cement (LC³) pastes in the context of digital concrete construction, in: *Rheol. Process. Constr. Mater.*, 2019, pp. 1–8.
- [133] C. Aramburo, C. Pedrajas, V. Rahhal, M. González, R. Talero, Calcined clays for low carbon cement: rheological behaviour in fresh Portland cement pastes, *Mater. Lett.* 239 (2019) 24–28, <https://doi.org/10.1016/j.matlet.2018.12.050>.
- [134] M.A.B. Beigh, V.N. Nerella, C. Schröfl, V. Mechtcherine, Studying the rheological behavior of limestone calcined clay cement (LC3) mixtures in the context of extrusion-based 3D-printing, in: S. Bishnoi (Ed.), *Calcined Clays Sustain. Concr.*, Springer Singapore, 2020, pp. 229–236, https://doi.org/10.1007/978-981-15-2806-4_26.
- [135] M. Chen, L. Yang, Y. Zheng, Y. Huang, L. Li, P. Zhao, S. Wang, L. Lu, X. Cheng, Yield stress and thixotropy control of 3D-printed calcium sulfoaluminate cement composites with metakaolin related to structural build-up, *Construct. Build. Mater.* 252 (2020) 119090, <https://doi.org/10.1016/j.conbuildmat.2020.119090>.
- [136] M. Bohuchval, M. Sonebi, S. Amziane, A. Perrot, Effect of metakaolin, and natural fibres on rheological properties of 3D printing concrete, *Proc. Inst. Civ. Eng. - Constr. Mater.* 19 (6) (2020) 1–34, <https://doi.org/10.1680/jcoma.20.00009>.
- [137] G. Ma, L. Wang, A critical review of preparation design and workability measurement of concrete material for largescale 3D printing, *Front. Struct. Civ. Eng.* 12 (2018) 382–400, <https://doi.org/10.1007/s11709-017-0430-x>.
- [138] H. Alghamdi, N. Neithalath, Synthesis and characterization of 3D-printable geopolymeric foams for thermally efficient building envelope materials, *Cement Concr. Compos.* 104 (2019) 103377, <https://doi.org/10.1016/j.cemconcomp.2019.103377>.
- [139] Y.W.D. Tay, Y. Qian, M.J. Tan, Printability region for 3D concrete printing using slump and slump flow test, *Compos. B Eng.* 174 (2019), <https://doi.org/10.1016/j.compositesb.2019.106968>.
- [140] B. Panda, M.J. Tan, Experimental study on mix proportion and fresh properties of fly ash based geopolymer for 3D concrete printing, *Ceram. Int.* 44 (2018) 10258–10265, <https://doi.org/10.1016/j.ceramint.2018.03.031>.
- [141] R.J. Flatt, D. Larosa, N. Rousset, Linking yield stress measurements: spread test versus Viskomat, *Cement Concr. Res.* 36 (2006) 99–109, <https://doi.org/10.1016/j.cemconres.2005.08.001>.
- [142] ASTM C1437-15, *Standard Test Method for Flow of Hydraulic Cement Mortar*, 2015, <https://doi.org/10.1520/C1437-15>.
- [143] A. Perrot, D. Rangeard, V. Nerella, V. Mechtcherine, Extrusion of cement-based materials - an overview, *RILEM Tech. Lett.* 3 (2019) 91–97, <https://doi.org/10.21809/rilemtechlett.2018.75>.
- [144] R. Alfani, G.L. Guerrini, Rheological test methods for the characterization of extrudable cement-based materials - a review, *Mater. Struct. Constr.* 38 (2005) 239–247, <https://doi.org/10.1617/14191>.
- [145] X. Zhou, Z. Li, Characterization of rheology of fresh fiber reinforced cementitious composites through ram extrusion, *Mater. Struct. Constr.* 38 (2005) 17–24, <https://doi.org/10.1617/14064>.
- [146] A. Perrot, Y. Mélinge, D. Rangeard, F. Micaelli, P. Estellé, C. Lanos, Use of ram extruder as a combined rheo-tribometer to study the behaviour of high yield stress fluids at low strain rate, *Rheol. Acta* 51 (2012) 743–754, <https://doi.org/10.1007/s00397-012-0638-6>.
- [147] Y. Chen, S. Chaves Figueiredo, Ç. Yalçınkaya, O. Çopuroğlu, F. Veer, E. Schlangen, The effect of viscosity-modifying admixture on the extrudability of limestone and calcined clay-based cementitious material for extrusion-based 3D concrete printing, *Materials* 12 (2019) 1374, <https://doi.org/10.3390/ma12091374>.
- [148] H. Ogura, V.N. Nerella, V. Mechtcherine, Developing and testing of strain-hardening cement-based composites (SHCC) in the context of 3D-printing, *Materials* 11 (2018) 1–18, <https://doi.org/10.3390/ma11081375>.
- [149] A. Pierre, A. Perrot, A. Histace, S. Gharsalli, E.H. Kadri, A study on the limitations of a vane rheometer for mineral suspensions using image processing, *Rheol. Acta* 56 (2017) 351–367, <https://doi.org/10.1007/s00397-017-0993-4>.
- [150] X. Zhou, Z. Li, M. Fan, H. Chen, Rheology of semi-solid fresh cement pastes and mortars in orifice extrusion, *Cement Concr. Compos.* 37 (2013) 304–311, <https://doi.org/10.1016/j.cemconcomp.2013.01.004>.
- [151] J.J. Benbow, J. Bridgwater, The influence of formulation on extrudate structure and strength, *Chem. Eng. Sci.* 42 (1987) 753–766, [https://doi.org/10.1016/0009-2509\(87\)80035-0](https://doi.org/10.1016/0009-2509(87)80035-0).
- [152] S. Chaves Figueiredo, O. Çopuroğlu, E. Schlangen, Effect of viscosity modifier admixture on Portland cement paste hydration and microstructure, *Construct. Build. Mater.* 212 (2019) 818–840, <https://doi.org/10.1016/j.conbuildmat.2019.04.020>.
- [153] R.A. Basterfield, C.J. Lawrence, M.J. Adams, On the interpretation of orifice extrusion data for viscoplastic materials, *Chem. Eng. Sci.* 60 (2005) 2599–2607, <https://doi.org/10.1016/j.ces.2004.12.019>.
- [154] P.R. Chhabra, J.F. Richardson, *Non-Newtonian Flow and Applied Rheology: Engineering Applications*, Cambridge University Press, Cambridge, 2008,

- <https://doi.org/10.1017/CBO9781107415324.004>.
- [155] V. Mechtcherine, V.N. Nerella, K. Kasten, Testing pumpability of concrete using sliding pipe rheometer, *Construct. Build. Mater.* 53 (2014) 312–323, <https://doi.org/10.1016/j.conbuildmat.2013.11.037>.
- [156] V.N. Nerella, V. Mechtcherine, Virtual sliding pipe rheometer for estimating pumpability of concrete, *Construct. Build. Mater.* 170 (2018) 366–377, <https://doi.org/10.1016/j.conbuildmat.2018.03.003>.
- [157] E. Secieriu, S. Fataei, C. Schröfl, V. Mechtcherine, Study on concrete pumpability combining different laboratory tools and linkage to rheology, *Construct. Build. Mater.* (2017), <https://doi.org/10.1016/j.conbuildmat.2017.03.199>.
- [158] V.N. Nerella, V. Mechtcherine, Studying the printability of fresh concrete for formwork-free concrete onsite 3D printing Technology (CONPrint3D), in: 3D Concr. Print. Technol., Elsevier Inc., 2019, pp. 333–347, <https://doi.org/10.1016/b978-0-12-815481-6.00016-6>.
- [159] T. Wangler, N. Roussel, F.P. Bos, T.A.M. Salet, R.J. Flatt, Digital concrete: a review, *Cement Concr. Res.* (2019), <https://doi.org/10.1016/j.cemconres.2019.105780>.
- [160] B. Panda, G.B. Singh, C. Unluer, M.J. Tan, Synthesis and characterization of one-part geopolymers for extrusion based 3D concrete printing, *J. Clean. Prod.* 220 (2019) 610–619, <https://doi.org/10.1016/j.jclepro.2019.02.185>.
- [161] T. Wangler, E. Lloret, L. Reiter, N. Hack, F. Gramazio, M. Kohler, M. Bernhardt, B. Dillenburger, J. Buchli, N. Roussel, R. Flatt, Digital concrete: opportunities and challenges, *RILEM Tech. Lett.* 1 (2016) 67, <https://doi.org/10.21809/rilemtechlett.2016.16>.
- [162] R.J.M. Wolfs, F.P. Bos, T.A.M. Salet, Triaxial compression testing on early age concrete for numerical analysis of 3D concrete printing, *Cement Concr. Compos.* (2019), <https://doi.org/10.1016/j.cemconcomp.2019.103344>.
- [163] R.J.M. Wolfs, A.S.J. Suiker, Structural failure during extrusion-based 3D printing processes, *Int. J. Adv. Manuf. Technol.* 104 (2019) 565–584, <https://doi.org/10.1007/s00170-019-03844-6>.
- [164] M.S. Khan, F. Sanchez, H. Zhou, 3-D printing of concrete: beyond horizons, *Cement Concr. Res.* 133 (2020) 106070, <https://doi.org/10.1016/j.cemconres.2020.106070>.
- [165] V.N. Nerella, M. Krause, V. Mechtcherine, Direct printing test for buildability of 3D-printable concrete considering economic viability, *Autom. Construct.* 109 (2020) 102986, <https://doi.org/10.1016/j.autcon.2019.102986>.
- [166] R.J.M. Wolfs, F.P. Bos, T.A.M. Salet, Early age mechanical behaviour of 3D printed concrete: numerical modelling and experimental testing, *Cement Concr. Res.* 106 (2018) 103–116, <https://doi.org/10.1016/j.cemconres.2018.02.001>.
- [167] A. Perrot, D. Rangeard, A. Pierre, Structural build-up of cement-based materials used for 3D-printing extrusion techniques, *Mater. Struct.* 49 (2016) 1213–1220, <https://doi.org/10.1617/s11527-015-0571-0>.
- [168] A.R. Arunothayan, B. Nematollahi, R. Ranade, S.H. Bong, J. Sanjayan, Development of 3D-printable ultra-high performance fiber-reinforced concrete for digital construction, *Construct. Build. Mater.* 257 (2020) 119546, <https://doi.org/10.1016/j.conbuildmat.2020.119546>.
- [169] T. Voigt, T. Malonn, S.P. Shah, Green and early age compressive strength of extruded cement mortar monitored with compression tests and ultrasonic techniques, *Cement Concr. Res.* 36 (2006) 858–867, <https://doi.org/10.1016/j.cemconres.2005.09.005>.
- [170] R.J.M. Wolfs, F.P. Bos, T.A.M. Salet, Correlation between destructive compression tests and non-destructive ultrasonic measurements on early age 3D printed concrete, *Construct. Build. Mater.* 181 (2018) 447–454, <https://doi.org/10.1016/j.conbuildmat.2018.06.060>.
- [171] Y. Chen, Ç. Yalçınkaya, O. Çopuroğlu, E. Schlangen, The effect of viscosity modifier agent on the early age strength of the limestone and calcined clay-based sustainable and 3D printable cementitious material, in: *Proc. 10th Int. Concr. Congr., Bursa Akademik Odalar Birliği*, 2019, pp. 242–250.
- [172] A. V. Rahul, M. Santhanam, Evaluating the printability of concretes containing lightweight coarse aggregates, *Cement Concr. Compos.* 109 (2020) 103570, <https://doi.org/10.1016/j.cemconcomp.2020.103570>.
- [173] L.K. Mettler, F.K. Wittel, R.J. Flatt, H.J. Herrmann, Evolution of strength and failure of SCC during early hydration, *Cement Concr. Res.* 89 (2016) 288–296, <https://doi.org/10.1016/j.cemconres.2016.09.004>.
- [174] L. Reiter, *Structural Build-Up for Digital Fabrication with Concrete - Materials, Methods and Processes*, ETH Zurich, 2019.
- [175] U. Pott, C. Ehm, C. Jakob, D. Stephan, Investigation of the early cement hydration with a new penetration test, rheometry and in-situ XRD, in: V. Mechtcherine, K. Khayat, E. Secieriu (Eds.), *RILEM Bookseries*, Springer, Cham, 2020, pp. 246–255, https://doi.org/10.1007/978-3-030-22566-7_29.
- [176] M. Rubio, M. Sonebi, S. Amziane, 3D printing of fibre cement-based materials: fresh and rheological performances, in: *Proc. 2nd ICBBM (PRO 119)*, 2017, pp. 284–291.
- [177] D. Lootens, P. Jousset, L. Martinie, N. Roussel, R.J. Flatt, Yield stress during setting of cement pastes from penetration tests, *Cement Concr. Res.* 39 (2009) 401–408, <https://doi.org/10.1016/j.cemconres.2009.01.012>.
- [178] Y. Weng, S. Ruan, M. Li, L. Mo, C. Unluer, M.J. Tan, S. Qian, Feasibility study on sustainable magnesium potassium phosphate cement paste for 3D printing, *Construct. Build. Mater.* 221 (2019) 595–603, <https://doi.org/10.1016/j.conbuildmat.2019.05.053>.
- [179] P. Shakor, S. Nejadi, G. Paul, A study into the effect of different nozzles shapes and fibre-reinforcement in 3D printed mortar, *Materials* 12 (2019), <https://doi.org/10.3390/MA12101708>.
- [180] M. Chen, L. Li, J. Wang, Y. Huang, S. Wang, P. Zhao, L. Lu, X. Cheng, Rheological parameters and building time of 3D printing sulphoaluminate cement paste modified by retarder and diatomite, *Construct. Build. Mater.* 234 (2020) 117391, <https://doi.org/10.1016/j.conbuildmat.2019.117391>.
- [181] B. Panda, C. Unluer, M.J. Tan, Extrusion and rheology characterization of geopolymer nanocomposites used in 3D printing, *Compos. B Eng.* 176 (2019) 107290, <https://doi.org/10.1016/j.compositesb.2019.107290>.
- [182] J.G. Sanjayan, B. Nematollahi, M. Xia, T. Marchment, Effect of surface moisture on inter-layer strength of 3D printed concrete, *Construct. Build. Mater.* 172 (2018) 468–475, <https://doi.org/10.1016/j.conbuildmat.2018.03.232>.
- [183] Y. Liao, X. Wei, Penetration resistance and electrical resistivity of cement paste with superplasticizer, *Mater. Struct. Constr.* 47 (2014) 563–570, <https://doi.org/10.1617/s11527-013-0079-4>.
- [184] G. Sant, C.F. Ferraris, J. Weiss, Rheological properties of cement pastes: a discussion of structure formation and mechanical property development, *Cement Concr. Res.* 38 (2008) 1286–1296, <https://doi.org/10.1016/j.cemconres.2008.06.008>.
- [185] U. Pott, C. Jakob, D. Jansen, J. Neubauer, D. Stephan, Investigation of the incompatibilities of cement and superplasticizers and their influence on the rheological behavior, *Materials* 13 (2020), <https://doi.org/10.3390/ma13040977>.
- [186] H. Sleiman, A. Perrot, S. Amziane, A new look at the measurement of cementitious paste setting by Vicat test, *Cement Concr. Res.* 40 (2010) 681–686, <https://doi.org/10.1016/j.cemconres.2009.12.001>.
- [187] G. Ma, Y. Li, L. Wang, J. Zhang, Z. Li, Real-time quantification of fresh and hardened mechanical property for 3D printing material by intellectualization with piezoelectric transducers, *Construct. Build. Mater.* 241 (2020) 117982, <https://doi.org/10.1016/j.conbuildmat.2019.117982>.
- [188] A. Szabo, L. Reiter, E. Lloret-Fritsch, F. Gramazio, M. Kohler, R.J. Flatt, Mastering yield stress evolution and formwork friction for smart dynamic casting, *Materials* 13 (2020), 2084, <https://doi.org/10.3390/ma13092084>.
- [189] V.N. Nerella, M.A.B. Beigh, S. Fataei, V. Mechtcherine, Strain-based approach for measuring structural build-up of cement pastes in the context of digital construction, *Cement Concr. Res.* 115 (2019) 530–544, <https://doi.org/10.1016/j.cemconres.2018.08.003>.
- [190] H.A. Barnes, J.O. Carnali, The vane-in-cup as a novel rheometer geometry for shear thinning and thixotropic materials, *J. Rheol.* 34 (1990) 841–866, <https://doi.org/10.1122/1.550103>.
- [191] G. Ovarlez, *Introduction to the Rheometry of Complex Suspensions*, Woodhead Publishing Limited, 2011, <https://doi.org/10.1016/B978-0-85709-028-7.50002-9>.
- [192] N. Roussel, H. Bessaies-Bey, S. Kawashima, D. Marchon, K. Vasilic, R. Wolfs, Recent advances on yield stress and elasticity of fresh cement-based materials, *Cement Concr. Res.* 124 (2019) 105798, <https://doi.org/10.1016/j.cemconres.2019.105798>.
- [193] D. Feys, R. Cepuritis, S. Jacobsen, K. Lesage, E. Secieriu, A. Yahia, Measuring rheological properties of cement pastes: most common techniques, procedures and challenges, *RILEM Tech. Lett.* 2 (2017) 129–135, <https://doi.org/10.21809/rilemtechlett.2017.43>.
- [194] N. Roussel, G. Ovarlez, S. Garrault, C. Brumaud, The origins of thixotropy of fresh cement pastes, *Cement Concr. Res.* 42 (2012) 148–157, <https://doi.org/10.1016/j.cemconres.2011.09.004>.

- [195] A. Yahia, S. Mantellato, R.J. Flatt, Concrete rheology, in: *Sci. Technol. Concr. Admixtures*, Elsevier, 2016, pp. 97–127, <https://doi.org/10.1016/B978-0-08-100693-1.00007-2>.
- [196] Y. Weng, DEVELOPMENT AND OPTIMIZATION OF 3D PRINTABLE CEMENTITIOUS COMPOSITES FOR PRINTING APPLICATIONS, 2019.
- [197] M. Chen, B. Liu, L. Li, L. Cao, Y. Huang, S. Wang, P. Zhao, L. Lu, X. Cheng, Rheological parameters, thixotropy and creep of 3D-printed calcium sulfoaluminate cement composites modified by bentonite, *Compos. B Eng.* 186 (2020) 107821, <https://doi.org/10.1016/j.compositesb.2020.107821>.
- [198] I. Ivanova, V. Mechtcherine, Possibilities and challenges of constant shear rate test for evaluation of structural build-up rate of cementitious materials, *Cement Concr. Res.* 130 (2020) 105974, <https://doi.org/10.1016/j.cemconres.2020.105974>.
- [199] D. Lowke, Thixotropy of SCC—a model describing the effect of particle packing and superplasticizer adsorption on thixotropic structural build-up of the mortar phase based on interparticle interactions, *Cement Concr. Res.* 104 (2018) 94–104, <https://doi.org/10.1016/j.cemconres.2017.11.004>.
- [200] Q. Yuan, D. Zhou, B. Li, H. Huang, C. Shi, Effect of mineral admixtures on the structural build-up of cement paste, *Construct. Build. Mater.* 160 (2018) 117–126, <https://doi.org/10.1016/j.conbuildmat.2017.11.050>.
- [201] F. Mahaut, S. Mokéddem, X. Chateau, N. Roussel, G. Ovarlez, Effect of coarse particle volume fraction on the yield stress and thixotropy of cementitious materials, *Cement Concr. Res.* 38 (2008) 1276–1285, <https://doi.org/10.1016/j.cemconres.2008.06.001>.
- [202] A. Perrot, T. Lecompte, H. Khelifi, C. Brumaud, J. Hot, N. Roussel, Yield stress and bleeding of fresh cement pastes, *Cement Concr. Res.* 42 (2012) 937–944, <https://doi.org/10.1016/j.cemconres.2012.03.015>.
- [203] Q. Yuan, D. Zhou, K.H. Khayat, D. Feys, C. Shi, On the measurement of evolution of structural build-up of cement paste with time by static yield stress test vs. small amplitude oscillatory shear test, *Cement Concr. Res.* 99 (2017) 183–189, <https://doi.org/10.1016/j.cemconres.2017.05.014>.
- [204] Q. Yuan, X. Lu, K.H. Khayat, D. Feys, C. Shi, Small amplitude oscillatory shear technique to evaluate structural build-up of cement paste, *Mater. Struct. Constr.* 50 (2017) 1–12, <https://doi.org/10.1617/s11527-016-0978-2>.
- [205] M.A. Moelini, M. Hosseini, A. Yahia, Effectiveness of the rheometric methods to evaluate the build-up of cementitious mortars used for 3D printing, *Construct. Build. Mater.* 257 (2020) 119551, <https://doi.org/10.1016/j.conbuildmat.2020.119551>.
- [206] T. Conte, M. Chaouche, Rheological behavior of cement pastes under large amplitude oscillatory shear, *Cement Concr. Res.* 89 (2016) 332–344, <https://doi.org/10.1016/j.cemconres.2016.07.014>.
- [207] V.N. Nerella, S. Hempel, V. Mechtcherine, Effects of layer-interface properties on mechanical performance of concrete elements produced by extrusion-based 3D-printing, *Construct. Build. Mater.* 205 (2019) 586–601, <https://doi.org/10.1016/j.conbuildmat.2019.01.235>.
- [208] J. Xiao, H. Liu, T. Ding, Finite element analysis on the anisotropic behavior of 3D printed concrete under compression and flexure, *Addit. Manuf.* (2020) 101712, <https://doi.org/10.1016/j.addma.2020.101712>.
- [209] J. Van Der Putten, M. Deprez, V. Cnudde, G. De Schutter, K. Van Tittelboom, Microstructural characterization of 3D printed cementitious materials, *Materials* 12 (2019) 2993, <https://doi.org/10.3390/ma12182993>.
- [210] E. Keita, H. Bessaies-Bey, W. Zuo, P. Belin, N. Roussel, Weak bond strength between successive layers in extrusion-based additive manufacturing: measurement and physical origin, *Cement Concr. Res.* 123 (2019) 105787, <https://doi.org/10.1016/j.cemconres.2019.105787>.
- [211] N. Roussel, F. Cussigh, Distinct-layer casting of SCC: the mechanical consequences of thixotropy, *Cement Concr. Res.* 38 (2008) 624–632, <https://doi.org/10.1016/j.cemconres.2007.09.023>.
- [212] B. Zareiyani, B. Khoshnevis, Effects of interlocking on interlayer adhesion and strength of structures in 3D printing of concrete, *Autom. Construct.* (2017), <https://doi.org/10.1016/j.autcon.2017.08.019>.
- [213] B. Panda, S.C. Paul, N.A.N. Mohamed, Y.W.D. Tay, M.J. Tan, Measurement of tensile bond strength of 3D printed geopolymer mortar, *Meas. J. Int. Meas. Confed.* 113 (2018) 108–116, <https://doi.org/10.1016/j.measurement.2017.08.051>.
- [214] T.T. Le, S.A. Austin, S. Lim, R.A. Buswell, R. Law, A.G.F. Gibb, T. Thorpe, Hardened properties of high-performance printing concrete, *Cement Concr. Res.* 42 (2012) 558–566, <https://doi.org/10.1016/j.cemconres.2011.12.003>.
- [215] J. Van Der Putten, G. De Schutter, K. Van Tittelboom, Surface modification as a technique to improve inter-layer bonding strength in 3D printed cementitious materials, *RILEM Tech. Lett.* 4 (2019) 33–38, <https://doi.org/10.21809/rilemtechlett.2019.84>.
- [216] T. Marchment, J. Sanjayan, M. Xia, Method of enhancing interlayer bond strength in construction scale 3D printing with mortar by effective bond area amplification, *Mater. Des.* 169 (2019) 107684, <https://doi.org/10.1016/j.matdes.2019.107684>.
- [217] Z.Y. Ahmed, F.P. Bos, M.C.A.J. Van Brunshot, T.A.M. Salet, F.P. Bos, M.C.A.J. Van Brunshot, T.A.M.S., On-, On-demand additive manufacturing of functionally graded concrete, *Virtual Phys. Prototyp.* (2020) 1–17, 0, <https://doi.org/10.1080/17452759.2019.1709009>.
- [218] A.L. van Overmeir, Designing an Interlayer Reinforcement Solution for Printable Strain-Hardening Cement-Based Composites: Practical Research on Various Bond Improvement Concepts, TU Delft, 2020.
- [219] G. Ma, N. Muhammad, L. Wang, F. Wang, A novel additive mortar leveraging internal curing for enhancing interlayer bonding of cementitious composite for 3D printing A novel additive mortar leveraging internal curing for enhancing interlayer bonding of cementitious composite for 3D printing, *Construct. Build. Mater.* 244 (2020) 118305, <https://doi.org/10.1016/j.conbuildmat.2020.118305>.
- [220] Y. Chen, O. Çopuroğlu, C.R. Rodriguez, F.F. de Mendonca Filho, E. Schlangen, Characterization of air-void systems in 3D printed cementitious materials using optical image scanning and X-ray computed tomography, *Mater. Char.* 173 (2021) 110948, <https://doi.org/10.1016/j.matchar.2021.110948>.
- [221] A. Das, Y. Song, S. Mantellato, T. Wangler, R.J. Flatt, D.A. Lange, Influence of pumping/extrusion on the air-void system of 3D printed concrete, in: F. Bos, S. Lucas, R. Wolfs, T.A.M. Salet (Eds.), *Second RILEM Int. Conf. Concr. Digit. Fabr. DC 2020*, Springer, Cham, 2020, pp. 417–427, https://doi.org/10.1007/978-3-030-49916-7_43.
- [222] P. Choi, J.H. Yeon, K.K. Yun, Air-void structure, strength, and permeability of wet-mix shotcrete before and after shotcreting operation: the influences of silica fume and air-entraining agent, *Cement Concr. Compos.* 70 (2016) 69–77, <https://doi.org/10.1016/j.cemconcomp.2016.03.012>.
- [223] ASTM C457-98, Standard Test Method for Microscopical Determination of Parameters of the Air-Void System in Hardened Concrete, 1998, <https://doi.org/10.1520/C0457-98>.
- [224] NEN-EN 480-11, Admixtures for Concrete, Mortar and Grout - Test Methods - Part 11: Determination of Air Void Characteristics in Hardened Concrete, (2005), 2005.
- [225] A. Koenig, Analysis of air voids in cementitious materials using micro X-ray computed tomography (μ XCT), *Construct. Build. Mater.* 244 (2020) 118313, <https://doi.org/10.1016/j.conbuildmat.2020.118313>.
- [226] S.Y. Chung, P. Sikora, T. Rucinska, D. Stephan, M. Abd Elrahman, Comparison of the pore size distributions of concretes with different air-entraining admixture dosages using 2D and 3D imaging approaches, *Mater. Char.* 162 (2020) 110182, <https://doi.org/10.1016/j.matchar.2020.110182>.
- [227] K.Y. Kim, T.S. Yun, J. Choo, D.H. Kang, H.S. Shin, Determination of air-void parameters of hardened cement-based materials using X-ray computed tomography, *Construct. Build. Mater.* 37 (2012) 93–101, <https://doi.org/10.1016/j.conbuildmat.2012.07.012>.
- [228] T.S. Yun, K.Y. Kim, J. Choo, D.H. Kang, Quantifying the distribution of paste-void spacing of hardened cement paste using X-ray computed tomography, *Mater. Char.* 73 (2012) 137–143, <https://doi.org/10.1016/j.matchar.2012.08.008>.
- [229] G. Sokhansafat, M. Moradian, M. Finnell, A. Behravan, M.T. Ley, C. Lucero, J. Weiss, Using X-ray computed tomography to investigate mortar subjected to freeze-thaw cycles, *Cement Concr. Compos.* 108 (2020) 103520, <https://doi.org/10.1016/j.cemconcomp.2020.103520>.
- [230] H. Lee, J.-H.J. Kim, J.-H. Moon, W.-W. Kim, E.-A. Seo, Correlation between pore characteristics and tensile bond strength of additive manufactured mortar using X-ray computed tomography, *Construct. Build. Mater.* 226 (2019) 712–720, <https://doi.org/10.1016/j.conbuildmat.2019.07.161>.